Biointerface Research in Applied Chemistry
Open-Access Journal (ISSN: 2069-5837)

Article
Volume 16, Issue 4, 2026, 111
https://doi.org/10.33263/BRIAC164.111

Pan-Cancer Bioinformatics and Drug-Repurposing Analysis of HYAL1 and HYAL2 as Potential Prognostic and Immunomodulatory Biomarkers

Nayan Kumar Sarkar [1], Roney Miah [2,3], Md. Shaon Mia [4], Md. Nazim Uddin [5,*]

[1] Department of Biomedical Engineering, Faculty of Applied Science and Technology, Islamic University, Kushtia-7003, Bangladesh
[2] Faculty of Industrial Sciences and Technology, Universiti Malaysia Pahang, Al-Sultan Abdullah, Lebuhraya Tun Khalil Yaakob, Kuantan, Pahang, 26300 Malaysia
[3] Bio Aromatic Research Center, Universiti Malaysia Pahang, Al-Sultan Abdullah, Lebuhraya Tun Khalil Yaakob, Kuantan, Pahang, 26300 Malaysia
[4] Department of Chemistry, University of Dhaka, Dhaka, 1000, Bangladesh
[5] Institute of Food Science and Technology, Bangladesh Council of Scientific and Industrial Research, Dhaka, 1205, Bangladesh
* Correspondence: nazimbiochem@bcsir.gov.bd;

Received: 11.12.2025; Accepted: 16.05.2026; Published: 15.08.2026

Abstract: HYAL1 and HYAL2 are the predominant mammalian hyaluronidases in somatic cells that are implicated in extracellular matrix remodeling and cancer biology. Their roles have not yet been systematically tackled in any comprehensive pan-cancer study. In this study, we investigated HYAL1 and HYAL2 in 33 types of cancer using public databases through TIMER 2.0, GEPIA 2, UALCAN, cBioPortal, and Kaplan–Meier Plotter. The expression profiles of the two genes were unique, and their mutation incidence was low. Significant differences in promoter methylation levels between cancerous and normal tissues were observed. Their expression was clinically relevant and related to overall survival in a cancer-type–specific manner: high expression was a risk factor for some cancers and a protective factor in other cancers like kidney cancer. Moreover, HYAL1 and HYAL2 showed tumor-specific correlations with infiltration of $CD8^+$ T cells, indicating impacts on the immune microenvironment. We conducted structure-based molecular docking using HYAL1 (PDB: 2PE4) and an AlphaFold model of HYAL2. Several FDA-approved drugs presented favorable binding affinities: HYAL1-selective (-10.775 kcal/mol, CHEMBL1200507), HYAL2-selective (-9.352 kcal/mol, CHEMBL1200455), and potential dual binders (-8.8/-8.1 kcal/mol) (CHEMBL58). Our preliminary data suggest HYAL1 and HYAL2 may function as context-dependent biomarkers associated with cancer prognosis and immune microenvironment characteristics. These docking results indicate that the identified compounds are potential candidates for further investigation. However, our comprehensive computational analyses provide insights into the potential roles of HYAL1 and HYAL2 across multiple cancers, but experimental and clinical studies are required to validate their biological functions and therapeutic relevance.

Keywords: cancer biology; HYAL1; HYAL2; pan-cancer study; immunotherapy; oncogenesis.

1. Introduction

Cancer is the uncontrolled growth of cells, which is the second leading cause of death globally. In 2022, approximately 20 million newly identified cases were detected, and unfortunately, 9.7 million people died from the disease [1,2]. Therefore, understanding molecular mechanisms and identifying reliable biomarkers are essential for improving cancer prevention and treatment. Bioinformatics allows pan-cancer studies of cancer-associated genes using publicly available datasets [3]. The Cancer Genome Atlas (TCGA) provides comprehensive genomic data enabling pan-cancer analyses [4,5].

To overcome stromal barriers and enhance treatment efficacy, recent advances in cancer biology have highlighted the therapeutic potential of targeting ECM components [6]. HYAL1 and HYAL2 are enzymes that break down Hyaluronic acid (HA) in the extracellular matrix (ECM), altering the tumor microenvironment (TME) to support tumor growth, metastasis, and drug resistance [7,8]. Enzymatic HA depletion and hyaluronidase-based approaches have gained increasing attention for ECM-modulating strategies [9]. A recent study demonstrates that targeted hyaluronidase delivery can improve chemotherapeutic penetration and enhance $CD8^+$ T-cell infiltration within solid tumors [10].

HYAL1 functions in lysosomes, whereas HYAL2 acts on the cell membrane, interacting with targets such as CD44 [11]. Despite limited research over the past five years, only a few studies have examined HYAL1 and HYAL2 [12] across various types of cancer. Most research has focused on them individually, and a comprehensive analysis of their role in multiple cancers is still lacking (e.g., in prostate, colon [13,14], and breast cancers [15–17]. Although hyaluronidases from vertebrate somatic tissues are highly significant, their function remains unclear. Hyaluronic acid, a key molecule of the ECM, performs a vital role in retaining water within the intervertebral disc (IVD), providing flexibility and shock absorption in the spine. When HA is degraded by hyaluronidases (HYALs), some resulting fragments have been shown to trigger an inflammatory [18] and metabolic degradation response in human IVD cells [19]. The HYAL1 and HYAL2 genes are identified at chromosome 3p21.3 [20–22]. Our research focused on HYAL1 and HYAL2 on chromosome 3p21.3 because of their specific roles in HA metabolism, substantial interactions with cancer development and immunological regulation in a pan-cancer analysis, and their previously reported association with several tumor-related genes [7]. They break down the bond between N-acetylglucosamine and glucuronic acid, producing HA-derived molecules [23]. These genes enhance HA breakdown within and outside cells, depending on the presence of CD44 [24]. These studies have shown that non-cancerous cells, such as chondrocytes, macrophages, and keratinocytes, can take in HA for degradation through plasma membrane-bound HA receptors [25]. In tumors, cancerous cells frequently express membrane-bound HYAL1, which enables them to break down secreted HA into fragments of approximately 20 kDa [26,27]. Tumor cells from cancer patients and experimental animal tumors have demonstrated that tumor cells regularly interact with myeloid cells, such as MDSCs and TAMs [28], to degrade extracellular HA [29]. These myeloid cells contain abundant endocytosed HA and overexpress HYAL1 compared with tumor cells [30]. Several analyses have demonstrated that HA fragments are internalized by receptor-mediated endocytosis via cell-surface HA receptors, such as CD44 and HARE/Stabilin-2, in normal, non-cancerous cells [31,32]. These genes broadly examine the biological hallmarks of various tumors and their clinical outcomes. Given the complexity of oncogenesis and the associated challenges in tumor treatment responses, it is imperative to perform a pan-cancer study to

identify driver genes of interest and examine their potential impact on clinical outcomes [33,34].

In our study, we demonstrate context-dependent patterns of differential protein expression, methylation, prognostic significance, and immune associations across multiple cancer types of HYAL1 and HYAL2. To make potential biomarkers of cancer biology, we hypothesize that dysregulation of these hyaluronidase enzymes contributes to tumor progression and immune microenvironment remodeling in a cancer-specific manner. Following this, we evaluate the druggability of these enzymes, HYAL1 and HYAL2, which may provide insights into potential therapeutic strategies. To date, no clinically approved inhibitors of HYAL1 or HYAL2 exist. Our computational drug repurposing approaches offer a practical strategy for identifying candidate compounds that may interact with these enzymes. We introduced a structure-based molecular docking approach further to elucidate the clinical value of our biomarker exploration. As no HYAL1 or HYAL2 inhibitor has been developed to a clinical stage, docking may provide a rational approach for assessing their druggability and potential repurposing lines. HYAL1 has a crystal structure determined experimentally (PDB: 2PE4) [2], but HYAL2 lacks crystallographic data and was modeled using AlphaFold, which achieves near-experimental accuracy across a variety of proteins [35]. The list of FDA-approved drugs was selected for the ligand library because they can be developed rapidly and evaluated clinically, given their established safety profiles and pharmacokinetic properties [36]. For docking, the Glide XP protocol [37,38], which has demonstrated high predictive performance for scoring and enrichment in virtual screening campaigns [39], was used.

Our study involved a comprehensive analysis of HYAL1 and HYAL2 across multiple cancers using TCGA, CPTAC, and other public datasets to evaluate their contribution to tumor progression and patient outcomes. We investigated gene expression, genetic alterations, DNA methylation, clinical prognosis, and immune infiltration to clarify the roles of HYAL1 and HYAL2 in cancer biology. Additionally, structure-based molecular docking of FDA-approved drugs was performed to assess the druggability of the HYAL1 and HYAL2 enzymes. Although our comprehensive computational pan-cancer analyses provide insights into the biological relevance of HYAL1 and HYAL2 in cancer, future experimental validation is needed to confirm their functional roles and potential therapeutic significance.

2. Materials and Methods

2.1. Data sources.

TCGA (https://cancergenome.nih.gov/), cBioPortal (https://www.cbioportal.org/), Kaplan-Meier Plotter (https://kmplot.com/analysis), UALCAN (https://ualcan.path.uab.edu/), TIMER2.0 (http://timer.cistrome.org/), and GEPIA2 (http://gepia2.cancer-pku.cn/#analysis).

2.2. Cancer sample information.

We have collected initial data for our systematic pan-cancer analysis of HYAL1 and HYAL2 from publicly available TCGA data. Supplementary Table S01 lists the names and corresponding acronyms of the 33 cancer types.

2.3. Gene expression analysis

TIMER v2.0 helps explore the associations between gene expression and tumor features in the TCGA database. We utilized Timer's Gene DE Module to compare the gene expression patterns of HYAL1 and HYAL2 across various tumor types and their corresponding standard tissues. To control for different hypothesis testing across different cancer types and immune cell comparisons, using the Benjamini–Hochberg false discovery rate (FDR) correction, p-values were adjusted. The results are explained using box plots, with statistical significance indicated by high star count (*: p-value < 0.05; **: p-value < 0.01; ***: p-value < 0.001) based on the Wilcoxon test. We also utilized the GEPIA 2 website to analyze the expression of HYAL1 and HYAL2 in various tumor stages (using log2 (TPM + 1) for log-scale) from the TCGA database [40,41].

2.4. Protein expression analysis.

The UALCAN database investigated HYAL1 and HYAL2 expression disparities between tumor and normal tissues. Additionally, UALCAN provides an approach for protein expression analysis utilizing CPTAC datasets. The significance level was established at p-value < 0.05 [42,43].

2.5. Survival analysis.

Using the "Survival Map" module on GEPIA2, we created a map showing the overall survival significance of HYAL1 and HYAL2 across 33 tumor types. We set threshold values using 50% and 50% cutoffs to separate high- and low-expression groups. We also used the "Survival Analysis" module on the GEPIA2 website to generate survival plots and performed a log-rank test to assess the reliability of the statistical findings [41,44].

2.6. DNA methylation analysis.

The UALCAN database was used to investigate the DNA methylation of HYAL1 and HYAL2 levels in both normal tissues and cancer samples. The UALCAN database provides TCGA methylation data that was generated from the Illumina HumanMethylation450 BeadChip platform. Each probe's methylation level, which is located within the promoter region (−1500 bp upstream to +500 bp downstream of the transcription start site), is represented by a beta value, which is determined as the methylated signal divided by the total number of methylated and unmethylated signals. The beta value falls between zero (unmethylated) and one (completely methylated) [45].

2.7. Survival prognosis analysis.

The KM-plotter is a highly advanced web server for survival analysis that performs all calculations in real time. It compares and provides a detailed analysis of two patient cohorts using a KM survival plot, calculates the HR, 95% estimation range, and log-rank p-value ($p < 0.05$). The KM plotter can evaluate the effect of 54,000 genes on survival across 21 forms of cancer, mostly using Affymetrix microarray data from TCGA databases. This tool determines the overall survival prognostic value through Kaplan-Meier survival curves and Cox proportional hazards regression models of HYAL1 and HYAL2 expression in 21 cancers [46,47].

2.8. Genetic alteration analysis.

We used the cBioPortal for cancer genomics v6.4.4 database to analyze the genetic alteration data of HYAL1 and HYAL2, which includes the frequency of alterations, types of mutations, and specific mutation sites. Using TCGA Pan-Cancer Atlas Studies datasets, we evaluated the frequency of different mutation types for HYAL1 and HYAL2 and examined alteration frequencies within the "Cancer Types Summary" module. Additionally, we utilized the "Mutations" module to generate a mutation site plot for both genes [3,48].

2.9. Clinical outcome analysis.

Using the "Immune-Gene" module on the TIMER2.0 website [40], we evaluated HYAL1 and HYAL2 expression and correlated it with immune infiltration in all TCGA tumors. The outcome module allowed us to determine the clinical significance of tumor immune subsets while accounting for multiple factors using a multivariable Cox proportional hazards model. We identified CD8+ T cells, macrophages, CD4+ T cells, and gamma delta T cells as key components of immune infiltration. We examined immune cell infiltration using various algorithms, including MCPCOUNTER, TIMER, QUANTISEQ, CIBERSORT, XCELL, CIBERSORT-ABS, and EPIC, and calculated immune infiltration scores. To determine partial correlation and p-values ($p < 0.05$), we applied the purity-adjusted Spearman's rank correlation test and created a heatmap, as well as the model formula (Surv (OS, EVENT) ~ Infiltrate + Age + Stage + HYAL1 + HYAL2), which was applied to present the results [49].

2.10. Immune infiltration.

We examined immune cell infiltration using TIMER2's Immune module, with the TIMER algorithm as an estimate of infiltration. This module visualizes the relationship between gene expression and immune infiltration levels across several cancer types. To control for multiple cancer type comparisons, p-values were adjusted using the Benjamini-Hochberg false discovery rate (FDR) correction, and $p < 0.05$ was considered statistically significant. However, tumor purity is an important confounding factor in this study, as most immune cell types negatively correlate with it. This study suggests that tumor purity and immune infiltration are negatively associated. Furthermore, TIMER2 analyzed correlations with HYAL1 and HYAL2 mRNA expression, cancer-associated fibroblast infiltration, and CD8+ T cell infiltration.

2.11. Molecular docking of HYAL1 and HYAL2.

The X-ray crystal structure of HYAL1 (PDB ID: 2PE4, resolution: 2.60 Å) was obtained from the Protein Data Bank [35], and the structure of HYAL2 was taken from the AlphaFold Protein Structure Database because no experimentally determined structural data are available for this protein yet [50]. The AlphaFold model was evaluated based on the predicted local distance difference test (pLDDT) confidence scores. The majority of residues within the catalytic region showed high confidence scores (>80) that indicate reliable structural prediction in functionally relevant regions. Therefore, the AlphaFold model was considered suitable for structure-based docking analysis of the HYAL2 catalytic pocket. Both proteins were prepared with the Protein Preparation Wizard, which performs: (i) bond order assignment, (ii) addition of missing hydrogens, side chains and loops, (iii) refinement of incomplete regions by Prime, (iv) removal of waters not involved in interactions, and generation of ionization and

tautomeric states for hetero groups; optimization of hydrogen bonding was used to minimize steric clashes; restrained minimization was set on heavy atoms 0.3 Å RMSD using the impref module with the OPLS3e force field [51,52].

The ligand dataset is a subset of the ChEMBL database containing only FDA-approved drugs with clinical status up to Phase IV. The ligands were prepared using LigPrep v3.1, which includes desalting, hydrogenization, possible ionization, and tautomeric states at physiological pH (7 ± 0.2) generated using Epik v2. 9. Energy minimization was performed using the OPLS3e force field, and the lowest-energy conformations were saved in Maestro format (.mae), used for docking studies [53]. In docking studies, receptor grids were generated at the putative catalytic pockets of both enzymes. For HYAL1 (PDB ID: 2PE4), no co-crystallized ligand is available in the crystal structure; therefore, the receptor grid was defined according to the reported catalytic pocket residues described in previous structural studies**.** The grid was centered on the active-site region containing Asp129 and Glu131**,** with grid center coordinates set at (37.299972, −15.350472, −20.637425) [54]. For HYAL2, no crystallographic structure containing a bound ligand or validated small-molecule reference inhibitor is currently available. Therefore, the receptor grid was generated based on the predicted catalytic residues reported in the literature and supported by FTMap analysis. The docking pocket was defined around key catalytic residues Asp133, Glu135, Arg138, and Tyr206**,** with the grid center coordinates set at (12.238250, −7.665482, −2.285232) [55]. Docking was performed with the Ligand Docking module using Standard Precision (SP, Rigid) and Extra Precision (XP, Flexible) protocols [56,57]. No restriction on position was added, and ligands were sampled in several possible grid orientations using Euler rotations. Compounds with the top-most negative docking scores were considered for further study.

3. Results and Discussion

3.1. Differential expression of HYAL1 and HYAL2 across cancers.

3.1.1. Expression profile and clinical relevance of HYAL1 in pan-cancer cohorts.

We analyzed the transcriptome data in Figure 1A from TCGA of both tumor and normal tissues to determine the expression level of HYAL1 across human tumors. HYAL1 is significantly overexpressed in various cancer types, including BRCA-Basal and BRCA-Her2, PRAD, PAAD, and KICH, and underexpressed in KIRC, LIHC, LUAD, and SKCM. HYAL1 expression was significantly upregulated in various tumors, such as BLCA, BRCA, ESCA, HNSC, KIRC, KIRP, LUAD, STAD, and THCA (all p-values < 0.05). However, HYAL1 gene expression was downregulated in certain types of colorectal cancer, suggesting that its function varies by cancer type. To determine if HYAL1 expression is linked to tumor development, we analyzed its expression at different cancer stages (Figure 1B). The results indicated significant differences in HYAL1 expression across tumor stages, with notable exceptions. Kidney tumors, for instance, showed strong correlations with KIRC ($F = 20.4$, $p = 1.58 \times 10^{\wedge -12}$) and KIRP ($F = 6.3$, $p = 0.000385$), with variation across stages. Similar patterns were observed in bladder, breast, and liver cancers.

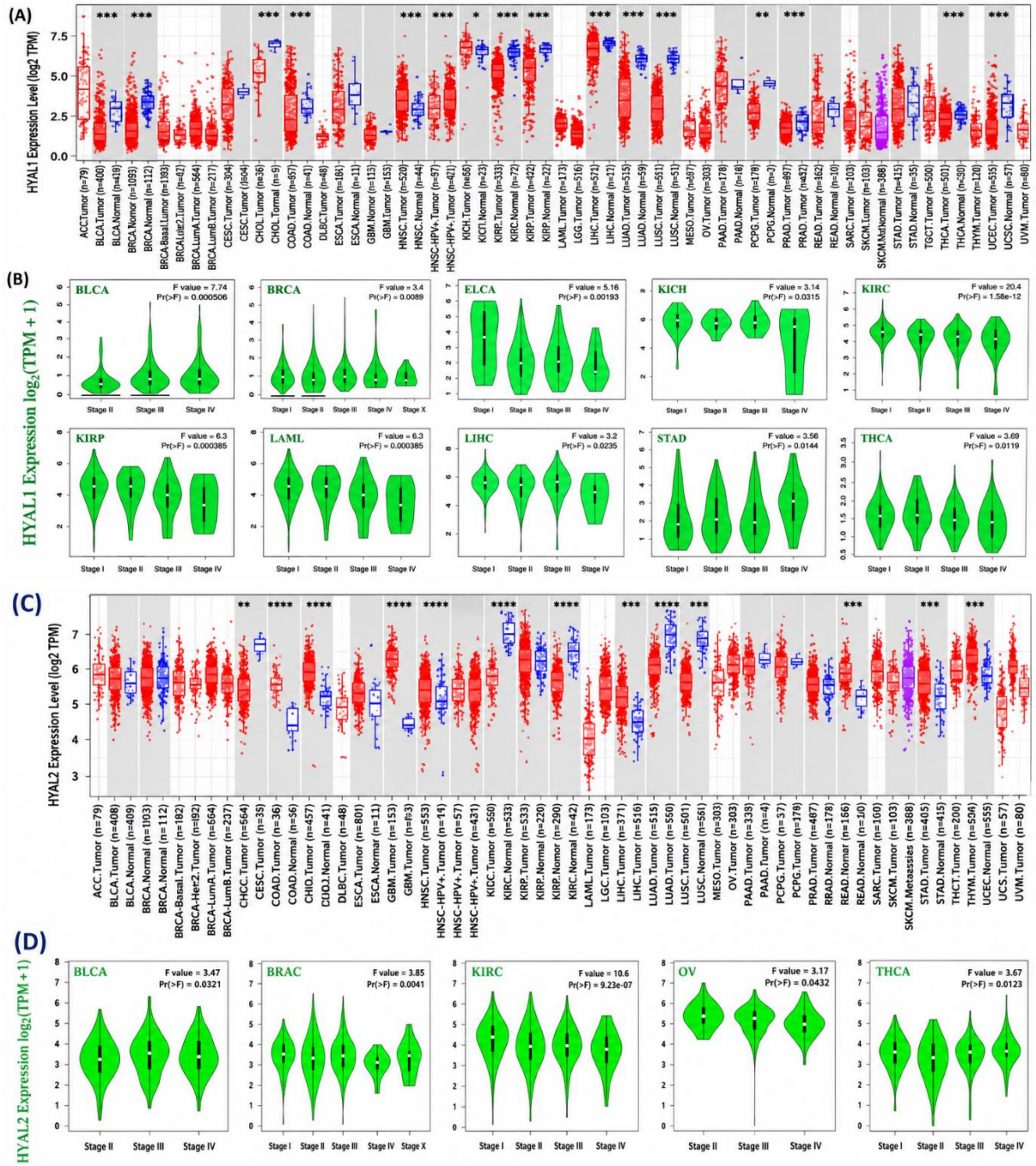

Figure 1. (A) represents the expression levels of HYAL1 in different cancers and clinical phases; **(B)** HYAL1 expression levels were compared across the primary pathological stages (stages I, II, III, and IV). Gene expression levels are presented as log2 (TPM + 1); **(C)** represents the expression levels of HYAL2 in different cancers and clinical phases; **(D)** HYAL2 expression levels were compared across the primary pathological stages (stages I, II, III, and IV). Gene expression levels are presented as log2 (TPM + 1).

3.1.2. Expression profile and clinical relevance of HYAL2 in pan-cancer cohorts.

Next, we analyzed the expression level of HYAL2 using the TCGA pan-cancer dataset (Figure 1C). Various types of tumors, including ESCA, HNSC, KIRC, LUAD, LUSC, and THCA, reveal a significant overexpression of HYAL2 in cancer tissues relative to normal controls (p-value < 0.001). HYAL2 is overexpressed in different tumors, including BRCA-Her2, BRCA-LumB, HNSC, KICH, and PRAD. In contrast, it is downregulated in BLCA, SKCM, and STAD. On the other hand, there was a notable decrease in HYAL2 gene expression in BLCA, BRCA, and COAD. We examined stage-specific expression patterns to determine if

HYAL2 expression is associated with clinical stage (Figure 1D). HYAL2 expression was significantly associated with tumor stage in KIRC ($F = 10.6$, $p = 9.23e{-}07$), BRCA ($F = 3.85$, $p = 0.0041$), BLCA ($F = 3.47$, $p = 0.0321$), OV ($F = 3.17$, $p = 0.0432$), and THCA ($F = 3.67$, $p = 0.0123$). Among these, KIRC showed significant stage-related variation, suggesting it is a potential stage-specific biomarker, especially in renal cancers.

3.2. Prognostic significance of HYAL1 and HYAL2.

Figure 2(A) illustrates the prognostic implications of survival analysis among several tumor types of HYAL1. In BLCA and KIRP, high HYAL1 expression is linked to adverse overall survival (OS) (log-rank p-value < 0.05), suggesting it may be a negative prognostic marker. On the other hand, in KIRC, high HYAL1 expression is associated with better overall survival, indicating a context-dependent tumor suppressor role. The heatmap above the survival curves highlights this trend, where red indicates a higher hazard ratio (HR), and blue shows a protective effect. These opposite survival associations suggest that HYAL1 functional impact may vary depending on the type of tumor, its environment, or the underlying molecular subgroups. Figure 2B presents a similar analysis for HYAL2, where high HYAL2 levels are associated with a poor prognosis in MESO and UVM (log-rank p-value < 0.05), as indicated by the KM plots and red HR tiles. In contrast, KIRC and LGG show better outcomes with higher HYAL2 expression. These patterns reinforce the dual nature of HYAL genes, which can be oncogenic or tumor suppressive. Figures 2(A) and 2(B) display KM survival plots that describe the OS probabilities across various cancer types. The curves are plotted with survival percentages on the y-axis (ranging from 0% to 100%) and time in months on the x-axis (spanning 0 to 200 months, depending on the cancer type). The data are grouped into two expression categories for each cancer type and analyzed for statistical significance. The red line indicates the High HYAL1 and HYAL2 group, whereas the blue line indicates the Low HYAL1 and HYAL2 group. P-values indicate significant differences in survival outcomes.

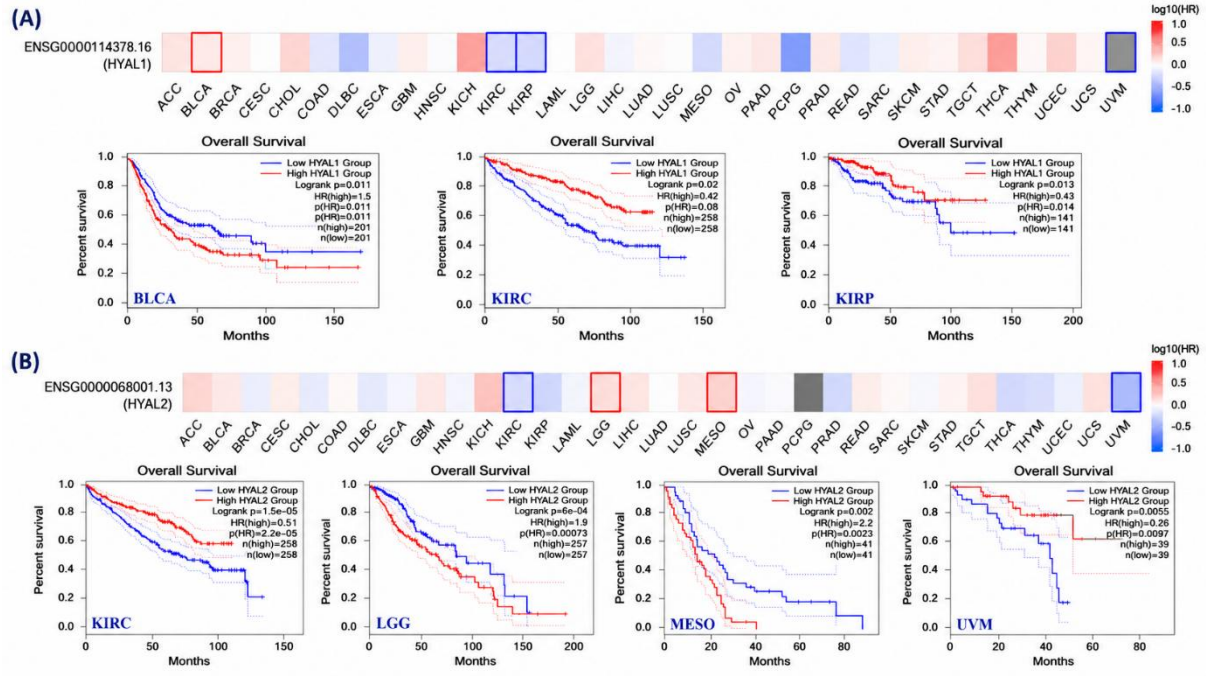

Figure 2. Survival analysis of (A) HYAL1 and (B) HYAL2 expression in various cancers. The Overall Survival (OS) maps illustrate the association between high and low gene expression levels and patient survival outcomes across different cancer types.

A color gradient bar at the top represents the log10 hazard ratio (HR < 1) correlation or ranking of expression levels across the cancer cohorts. Figure 2(A) displays survival curves for cancer types, including BLCA, KIRC, and KIRP. Figure 2(B) shows survival curves for various cancer types, including KIRC, LGG, MESO, and UVM.

3.3. Protein expression analysis.

Our results represent a box plot of HYAL1 and HYAL2 protein expression across various cancer types, utilizing CPTAC data. Figure 3(A) reveals that HYAL1 protein expression is significantly lower in tumor tissues compared to normal tissues, with adjusted low p-values (BRCA: p=1.7122E-05, KIRC: p=4.0115E-28, LUAD: p=3.1434E-11, LUSC: p=2.83603736973182E-42, HNSC: p=1.579581E-03, and LIHC: p=7.86934149170824E-18), indicating strong statistical significance. Figure 3(B) presents similar findings for HYAL2 protein expression across various malignancies, showing that HYAL2 expression is also increased in primary cancer samples compared to normal cells in BRCA and KIRC, but decreased in LUAD, LUSC, and HNSC. The statistical significance remains substantial (BRAC: p=1E-12, KIRC: p=3.77316260739804E-05, LUAD: p=1.4579E-22, LUSC: p=1.2874E-34, HNSC: p=1.381048E-04), supporting the idea that both HYAL1 and HYAL2 show significant differential expression across distinct tumor types.

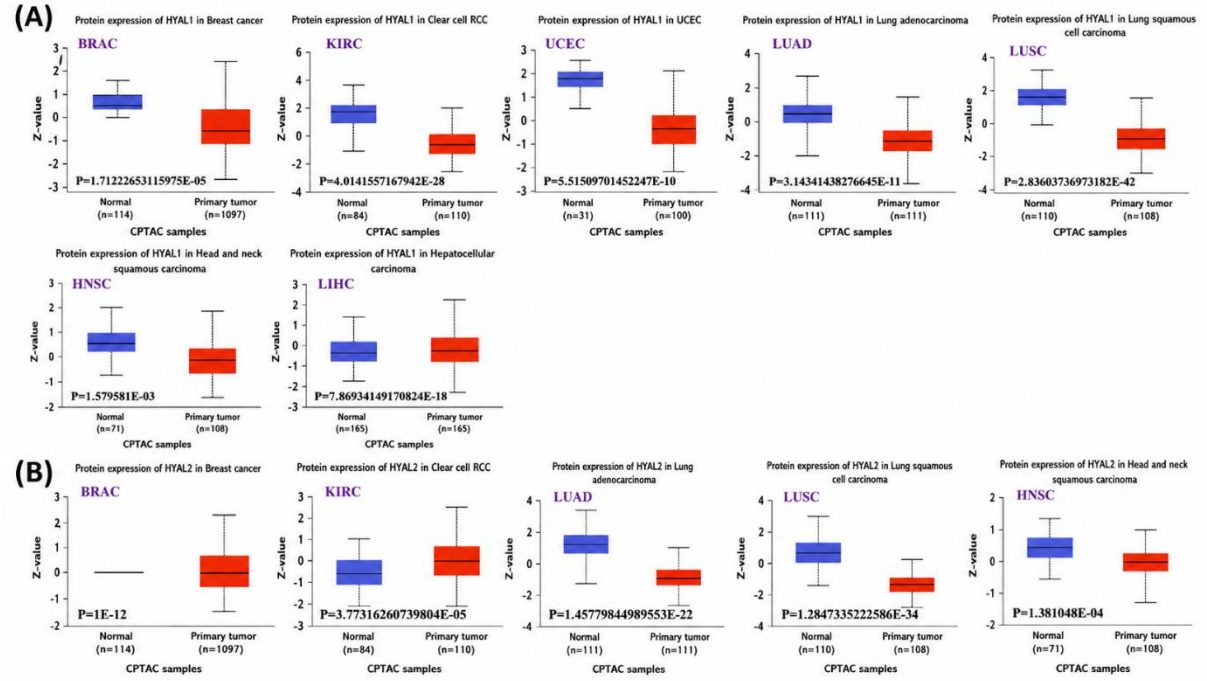

Figure 3. Protein expression levels of HYAL1 and HYAL2 across various cancer types based on CPTAC data. **(A)** shows HYAL1 protein expression; **(B)** shows HYAL2 protein expression.

3.4. Genetic alterations and mutational landscape of HYAL1 and HYAL2.

The findings reveal genetic changes in HYAL1 and HYAL2 genes in various tumors, employing observations from the TCGA database. Figures 4(A) and 4(C) show alteration frequencies of HYAL1 and HYAL2 across 10,967 samples from 10,953 patients. Both genes have low frequencies of alterations, with approximately 1% of patients in HYAL1 and 1.4% in HYAL2 exhibiting genetic alterations. These include mutations (green), amplifications (red), and deep deletions (blue), with higher alteration rates in certain cancers, like uterine corpus endometrial carcinoma and cutaneous melanoma. For HYAL1, amplifications and deep

deletions contribute to the observed alterations across multiple cancer types (OV, BLCA, and LIHC), although the overall alteration frequency remains low. Similarly, HYAL2 may exhibit a pattern similar to that of OV and BLCA cancers, with deep deletions less common but still observed in LUAD and LUSC.

Figures 4(B) and 4(D) present lollipop plots of somatic mutation distributions in the HYAL1 and HYAL2 protein sequences. HYAL1 has a somatic mutation frequency of 0.5%, with mutations distributed throughout its amino acid sequence, including the A311V variant. At the same time, HYAL2 shows a higher mutation frequency (0.6%), with R234S being the most prominent variant. Both mutations likely affect enzymatic function, which is key to ECM degradation. This disruption in enzymatic expression can enhance invasive potential, migration, and metastasis. Moreover, variants of uncertain significance (VUS) underscore the need for further experimental validation to determine their roles in tumor aggressiveness and patient prognosis. This study suggests that HYAL1 and HYAL2 are not typically altered in cancer but exhibit recurring genetic changes, particularly in specific cancer subtypes. This study supports the potential significance of HYAL1 and HYAL2 in cancer biology and may highlight the need for further research into their functional roles and therapeutic potential.

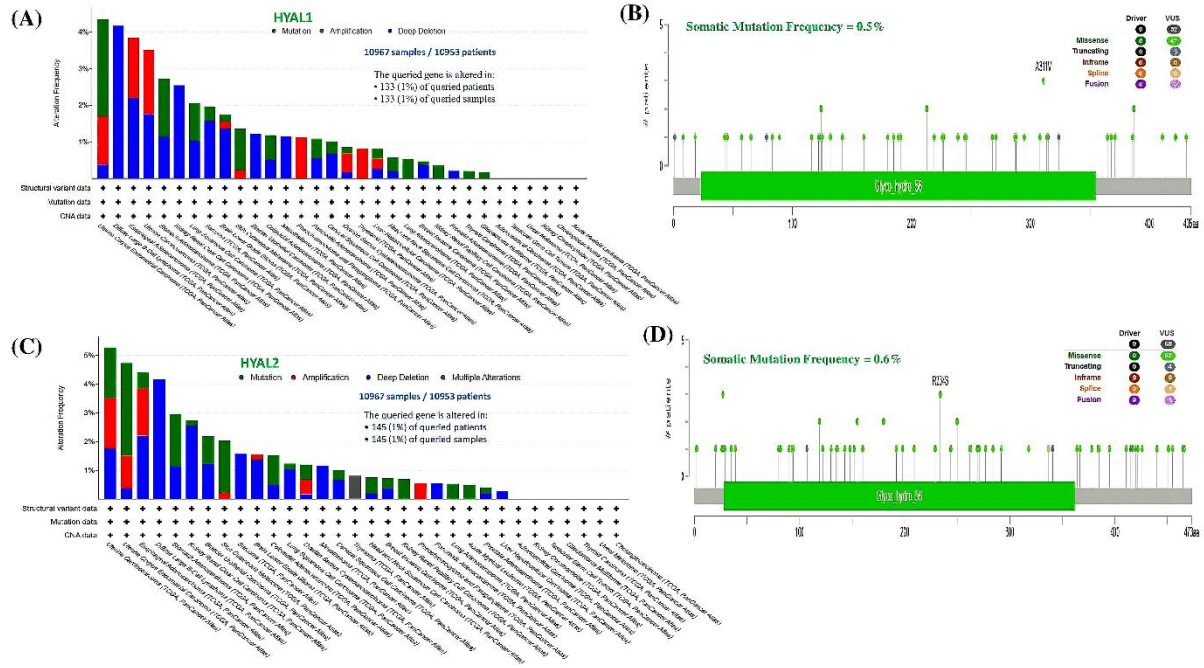

Figure 4. Mutation profiles of HYAL1 and HYAL2 in various TCGA cancers. **(A)** Alteration frequency; **(B)** Sites of various mutation types in all TCGA HYAL1 cancers; **(C)** The frequency of alterations; **(D)** the locations of various mutation types in all TCGA HYAL2 tumors.

3.5. Promoter methylation analysis of HYAL1 and HYAL2.

These findings show the promoter methylation levels for the HYAL1 and HYAL2 genes across various cancer types, with statistical significance highlighted by p-values. To evaluate the relationship between promoter methylation and transcriptional activity, Spearman correlation analysis was performed between methylation beta values and mRNA expression levels of HYAL1 and HYAL2 across TCGA cancers. Several cancer types showed increased promoter methylation associated with reduced gene expression, indicating a moderate negative Spearman correlation coefficient ($\rho < 0$). Finally, the statistical significance of these correlations was evaluated using Benjamini–Hochberg FDR correction, with p-values < 0.05 considered significant.

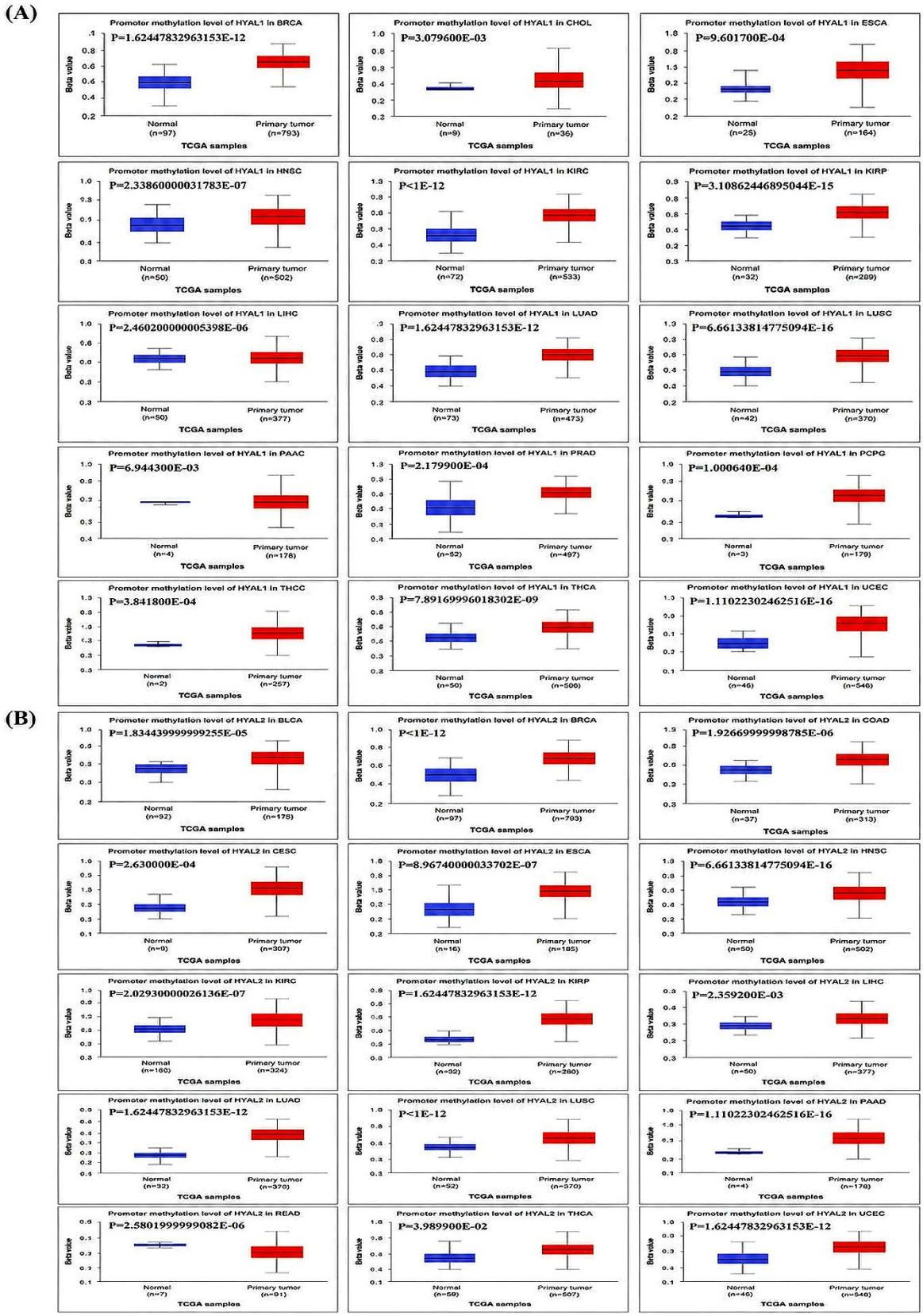

Figure 5. The methylation of the (A) HYAL1 and (B) HYAL2 genes in normal and cancerous cells. Significant differences in promoter methylation levels were observed between normal and tumor tissues for both HYAL1 and HYAL2 ($p < 0.05$).

In Figure 5(A), examining HYAL1 methylation, BRCA has a p-value of 1.624783293153e-12, ESCA a p-value of 9.601700e-04, KIRC a p-value of <1e-12, KIRP a p-value of 3.10624689054e-14, CHOL a p-value of 9.6070e-04, HNSC a p-value of

2.238600031783e-07, LIHC a p-value of 2.46020000005398e-06, LUAD a p-value of 1.624478326153e-12, LUSC a p-value of 6.663381475094e-16, PRAD a p-value of 2.17900e-04, PAAD a p-value of 6.944300e-03, READ a p-value of 1.00640e-04, THCA a p-value of 7.89169996018302e-09, SARC a p-value of 3.41800e-04, and UCEC a p-value of 1.1102230262516e-16. In Figure 5(B), for HYAL2 methylation, BRCA shows a p-value of 1.83439999255e-05, BLCA a p-value of 1.83443999999255e-05, CESC a p-value of 1.92669998785e-06, COAD a p-value of 1.92669999998785e-06, HNSC a p-value of 6.663381475094e-16, ESCA a p-value of 8.96740000033702e-07, KIRC a p-value of 2.02930000026136e-07, KIRP a p-value of 2.0293000e-07, LIHC a p-value of 1.624478326153e-12, LUAD a p-value of 1.624478326153e-12, LUSC a p-value of 1e-12, PRAD a p-value of 1.10232026516e-16, THCA a p-value of 3.989900e-02, READ a p-value of 2.58019999908e-06, and UCEC a p-value of 1.624478326153e-12. These p-values indicate that the methylation profiles of HYAL1 and HYAL2 differ significantly between normal and primary tumor samples across cancer types. The box plots, where red represents primary tumor samples and blue represents reference samples, indicate substantial changes in methylation profiles. This box plot demonstrates that epigenetic regulation of HYAL1 and HYAL2 may play an essential role in the development of these cancers, potentially providing valuable insights for diagnostic and therapeutic approaches.

3.6. Prognostic role of HYAL1 and HYAL2 in different cancers.

These findings describe KM survival curves that examine patients' overall survival rates according to HYAL1 and HYAL2 expression levels among different types of cancer. The survival curves for HYAL1 expression show a consistent link between higher expression and better overall survival across multiple tumor types.

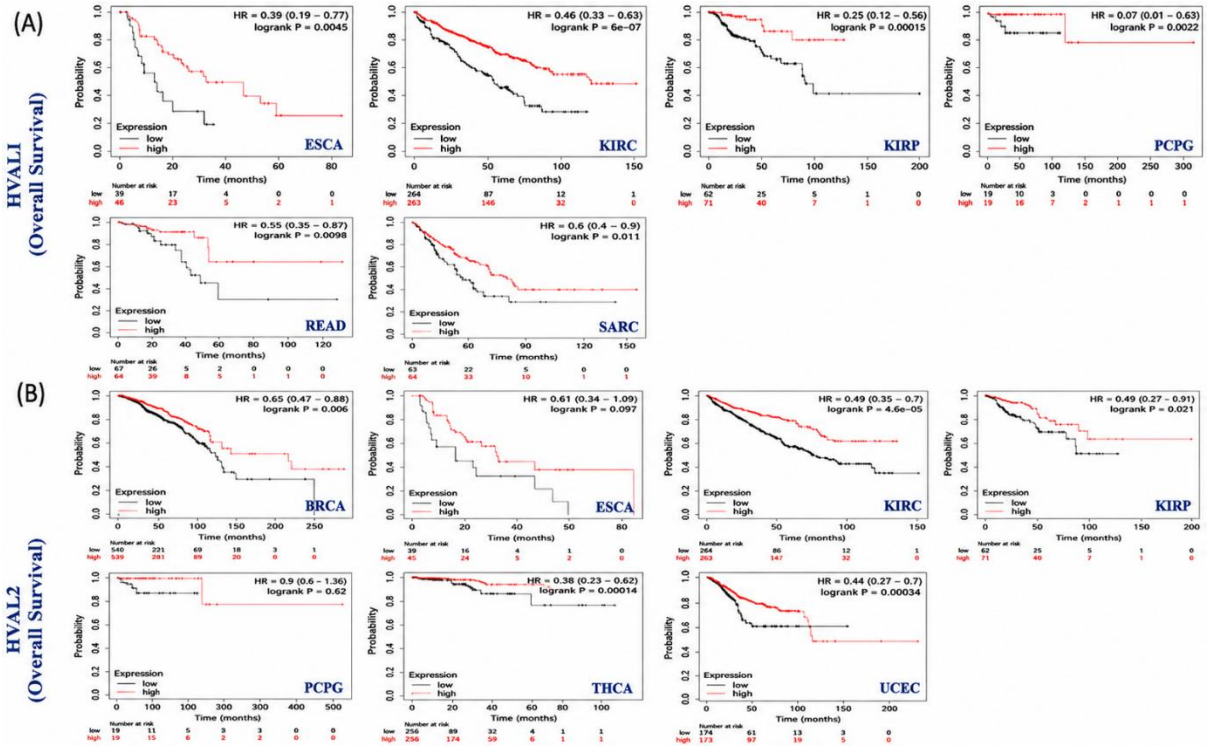

Figure 6. Overall survival curves for tumors with low and high (A) HYAL1 and (B) HYAL2 expression levels. Significant associations were observed between HYAL1 and HYAL2 expression levels and patient overall survival ($p < 0.05$).

Specifically, we found a hazard ratio of 0.39 (p = 0. 0055) for ESCA, 0.46 (p = 4 e-07) for KIRC, 0.25 (p = 0.00015) for KIRP, 0.07 (p = 0. 0022) for PCPG, 0.35 (p = 0. 0063) for READ, and 0.6 (p = 0.015) for SARC. The statistically significant p-values (P < 0.05) and hazard ratios (HRs) less than 1 suggest that HYAL1 may be a promising pan-cancer prognostic biomarker (Figure 6A). Higher expression levels are associated with a reduced risk of death across multiple cancer types, underscoring the need for further research into the molecular processes that control HYAL1 and its role in cancer development. The survival curves for HYAL2 expression demonstrate a relationship between higher expression levels and improved OS. The hazard ratios (HRs) and p- values were as follows: BRCA had an HR of 0. 65 (p = 0. 007), ESCA had an HR of 0. 46 (p = 0. 017), KIRC had an HR of 0. 49 (p = 0. 00025), KIRP had an HR of 0. 49 (p = 0. 018), PCPG had an HR of 0 (p = 0. 002), THCA had an HR of 0. 28 (p = 0. 0084), and UCEC had an HR of 0. 58 (p = 0. 014) (Figure 6B). HYAL2's consistent significance across various cancer types suggests it may also serve as a potential pan-cancer prognostic biomarker. The findings indicate that higher expression of HYAL1 and HYAL2 is consistently associated with better survival, with statistically significant hazard ratios (HRs) and p-values reported across most cancer types. These results indicate that high expression levels of HYAL1 and HYAL2 are associated with favorable OS across various cancer types, with substantial p-values confirming their prognostic significance.

3.7. Gene outcome analysis of HYAL1 and HYAL2 expression

Based on gene outcome analysis using the TIMER2.0 website, KM survival curves illustrate the effect of HYAL1 and HYAL2 expression on OS across various cancer types.

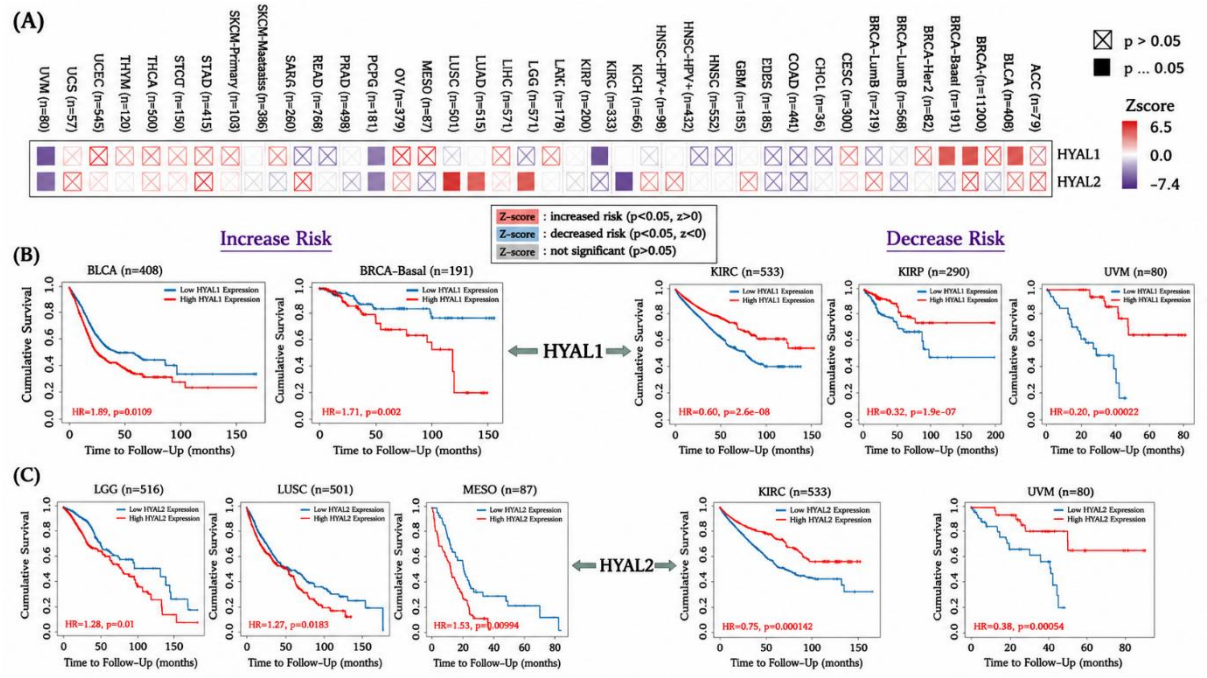

Figure 7. Prognostic Impact of HYAL1 and HYAL2 Expression on Overall Survival across Multiple Cancer Types (A) Heatmap displaying Z-scores of HYAL1 and HYAL2 expression related to overall survival across various cancers. Red indicates increased risk (Z > 0.5) while blue indicates decreased risk (Z < -0.4), with noted statistical significance (p-value < 0.05). The KM survival curves for (B) HYAL1 and (C) HYAL2 expressions in selected cancers.

Figure 7(A) is a heatmap of Z-scores for HYAL1 and HYAL2 expression in cancers from TCGA, where red indicates a higher risk (Z-score > 0.5), and blue indicates a lower risk (Z-score < -0.4), with statistical significance (p < 0.05). HYAL1 is associated with a higher

risk in cancers like BLCA (HR = 1.18 and p = 0.0293) and BRCA-Basal (HR = 1.51 and p = 0.0333), but a lower risk in KIRC (HR = 0.735 and p = 2.41e-05), KIRP (HR = 0.609 and p = 0.00137), and UVM (HR = 0.276 and p = 0.000123). HYAL2 also shows cancer-type-specific patterns, increasing risk in MESO (HR = 1.53 and p = 0.000994), LGG (HR = 1.26 and p = 0.01), and LUSC (HR = 1.17 and p = 0.0183), but providing protection in KIRC (HR = 0.757 and p = 0.000142) and UVM (HR = 0.389 and p = 0.000654). Figure 7(B) presents KM survival curves for HYAL1 expression in selected cancers. In BLCA and BRCA-Basal, high HYAL1 expression is linked to significantly worse overall survival, indicating a higher patient risk. In contrast, in KIRC, KIRP, and UVM, high HYAL1 expression significantly correlates with improved survival as a protective factor in these cancer types. Figure 7(C) illustrates survival outcomes based on HYAL2 expression. High HYAL2 levels are associated with a poor prognosis in LGG, LUSC, and MESO, whereas in KIRC and UVM, higher expression is associated with significantly better survival outcomes. The data suggest that HYAL1 and HYAL2 are potential prognostic biomarkers, with their effects highly dependent on tumor context. Their differential impact on survival outcomes across cancer types underscores their potential to guide personalized therapeutic strategies.

3.8. Immune microenvironment of HYAL1 and HYAL2.

Figure 8 and Supplementary Figures S02 and S03 analyze the correlation between the expression levels of HYAL1 and HYAL2 and immune cell infiltration (specifically CD8+ T cells) across various cancer types using the TIMER 2.0 database. It presents heat maps that summarize the correlation between HYAL1 and HYAL2 expression and CD8+ T-cell infiltration across multiple types of tumors. These correlations are assessed using Spearman's partial correlation, adjusting for tumor purity, as well as using the Benjamini–Hochberg FDR correction. All statistical significance reported in the immune infiltration analysis was adjusted for multiple comparisons across cancer types. The intensity of the color denotes the strength and direction of the correlation: A positive correlation is denoted by red ($p<0.05$, $p>0$), where blue indicates a negative correlation ($p<0.05$, $p<0$), and gray boxes marked with an "X" denote non-significant correlations ($p>0.05$). Both genes HYAL1 and HYAL2 demonstrate significant positive and negative associations across various cancers. Supplementary Figures S02 and S03 present scatter plots illustrating the correlation levels of HYAL1 and HYAL2 expression and CD8+ T_EPIC cell infiltration in selected cancer types, categorized into positive and negative correlations. From Supplementary Figure S02, in ESCA, HNSC-HPV-, LGG, READ, TGCT, and THCA, HYAL1 expression displays a statistically significant positive correlation with CD8+ T_EPIC cell infiltration, indicating a potential role in promoting immune cell recruitment. In contrast, cancers such as CHOL, HNSC-HPV+, THYM, and UVM exhibit a negative correlation, suggesting that elevated HYAL1 expression may be associated with reduced immune infiltration. Supplementary Figure S03 displays analogous scatter plots for HYAL2, categorized by positive and negative correlations. HYAL2 expression reveals strong positive correlations with CD8+ T_EPIC cell infiltration in several cancers, including BLCA, CESC, KIRP, PRAD, and THCA, suggesting an immune-promoting role. Conversely, negative correlations are observed in cancers such as BRCA, BRCA-Basal, BRCA-Her2, BRCA-Lumb, COACD, HNSC, HNSC-HPV-, MESO, PCPG, SARC, SKCM, SKCM-Metastasis, THYM, and UVM, suggesting a potential association between high HYAL2 expression and reduced immune cell presence. This figure illustrates the immunomodulatory functions of HYAL1 and HYAL2 within the tumor microenvironment. The expression levels of both genes are

significantly correlated with CD8+ T cell infiltration in a cancer-specific manner, with HYAL1 and HYAL2 demonstrating a broader pattern of context-dependent immune associations rather than uniformly positive immune associations. These findings suggest that HYAL1 and HYAL2 may influence anti-tumor immunity and be prospective biomarkers for immuno-oncology.

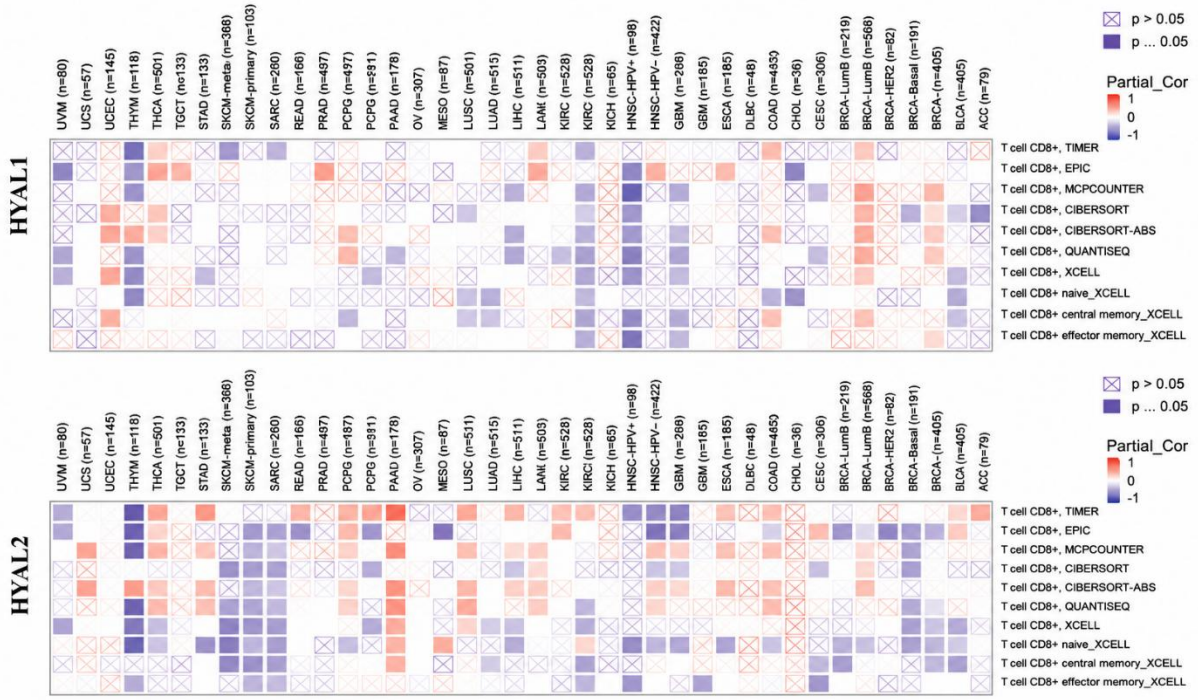

Figure 8. Correlation analysis of HYAL1 and HYAL2 expression with immune infiltration.

3.9. Molecular docking analysis of HYAL1 and HYAL2.

Molecular docking studies by the Schrödinger Glide XP protocol were conducted to predict the inhibition of FDA-approved molecules on active sites of catalytic domains of HYAL1 and HYAL2 (Tables 1 and 2). The detailed docking results for all compounds are included in the Supplementary Data Table 2. Here, the four best-performing compounds for each target are presented, comprising two dual inhibitors and two target-selective compounds, along with their docking scores and key interaction profiles.

Table 1. Molecular docking results of selected compounds against HYAL1, showing XP docking scores and key protein–ligand interactions.

CHEMBL ID	Drug name	HYAL1 XP score (kcal/mol)	Ligand efficiency	Interaction profiles	Type
	Glycyrrhizin	−6.379	0.110	Conventional H-bond: Arg134 (2.84 Å), Glu131 (3.02 Å), Thr143 (2.93 Å), Lys144 (3.19 Å); charge–charge interaction with Arg134; π–sigma / π–alkyl interactions with Tyr75 and Trp321	Reference inhibitor
CHEMBL 1200507	IODIXANOL	-10.8	0.174	Conventional H-bond: Asp142 (2.60 Å), Thr143 (2.82 Å), Lys144 (2.88 Å), Tyr84 (3.19 Å), Tyr85 (3.36 Å), Glu131 (3.08 Å); Carbon H-bond: Asp206 (3.58 Å); Alkyl interaction: Pro87 (4.03 Å)	HYAL1 selective
CHEMBL 1095607	REPROTEROL	-9.7	0.345	Conventional H-bond: Trp324 (3.12 Å), Asn39 (2.89 Å), Val322 (3.08 Å); π–π stacked: Trp324 (4.89 Å); π–π T-shaped: Trp321 (5.44 Å); π-alkyl: Pro62 (4.32 Å); Charge interaction: Glu131 (4.45 Å)	HYAL1 selective
CHEMBL 1200647	CANDICIDIN	-10.4	0.097	Conventional H-bond: Glu131 (2.68 Å), Ser76 (2.77 Å), Tyr75 (3.03 Å), Thr86	Dual

CHEMBL ID	Drug name	HYAL1 XP score (kcal/mol)	Ligand efficiency	Interaction profiles	Type
				(3.37 Å); Salt bridge: Glu131 (2.74 Å); Charge–charge interaction: Lys144 (3.66 Å); π-alkyl: Tyr147 (5.49 Å); π-sigma: Tyr75 (3.93 Å)	
CHEMBL 58	MITOXANTRONE	-8.3	0.226	Conventional H-bond: Glu131 (2.60 Å), Ser76 (2.66 Å), Val322 (2.72 Å); Salt bridge: Glu131 (2.84 Å); π–π stacked: Trp324 (4.27 Å); π–π T-shaped: Trp324 (5.46 Å); π-alkyl: Pro62 (4.10 Å)	Dual

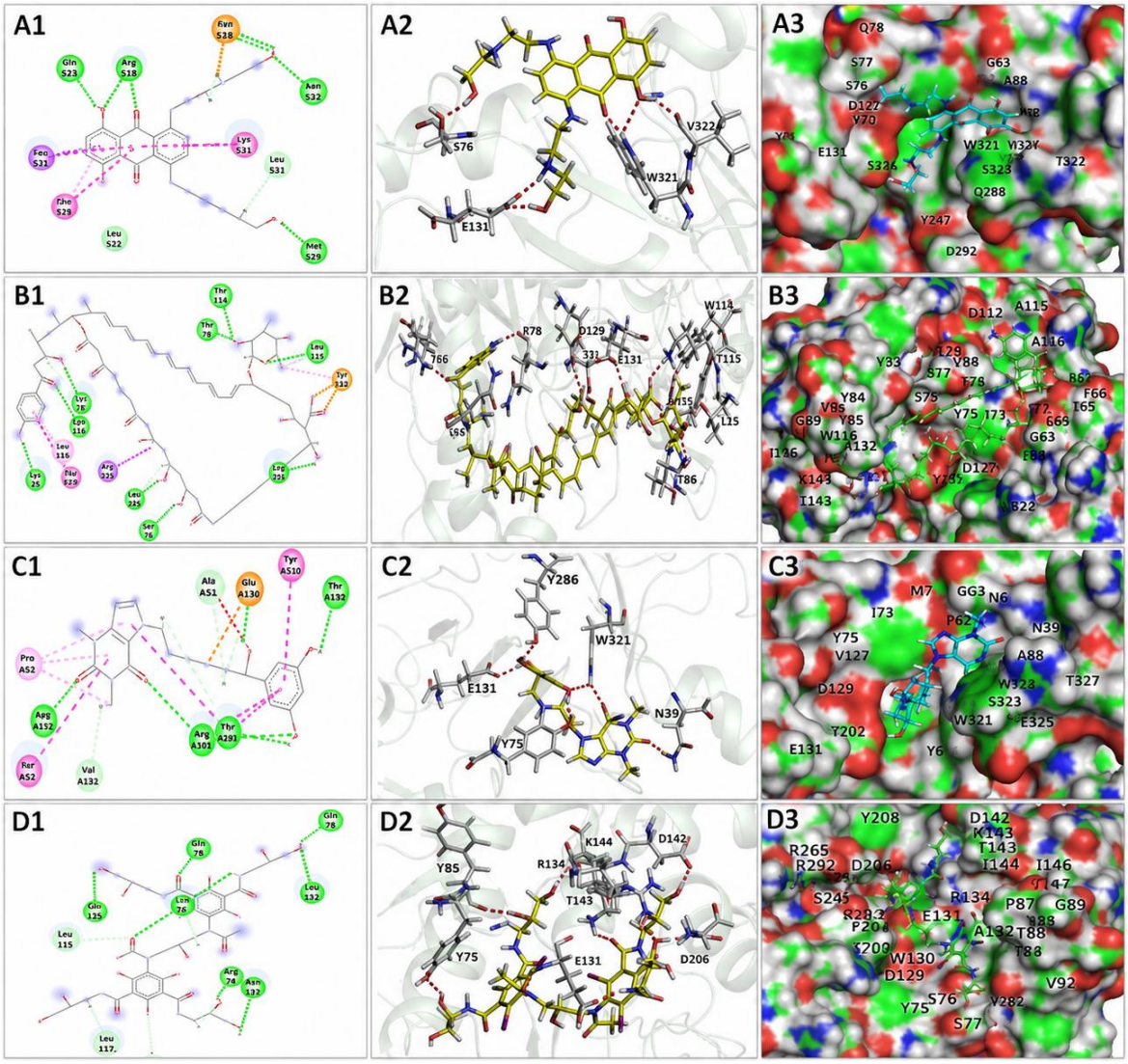

Figure 9. Molecular docking interactions of HYAL1 with FDA-approved ligands. (A) Mitoxantrone (CHEMBL58) and (B) Candicidin (CHEMBL1200647) show binding to conserved catalytic residues of HYAL1. (C) Iodixanol (CHEMBL1200507) and (D) Reproterol (CHEMBL1095607) represent HYAL1-selective ligands and exhibit isoform-specific interactions with the protein.

Table 2. Molecular docking results of selected drugs against HYAL2, showing XP docking scores and detailed protein–ligand interaction profiles.

CHEMBL ID	Drug name	HYAL2 XP score (kcal/mol)	Ligand efficiency	Interaction profiles	Type
CHEMBL1200455	IOHEXOL	-9.352	0.275	Conventional H-bond: Asp136 (2.69 Å), Asp133 (2.91 Å), Tyr79 (3.02 Å), Glu68 (2.79 Å); π–π stacked: Tyr79 (4.37 Å); π-alkyl: Pro66 (2.93 Å)	HYAL2 selective
CHEMBL1201075	IOXILAN	-8.868	0.277	Conventional H-bond: Glu135 (3.14 Å), Asp136 (3.39 Å), Tyr79	HYAL2 selective

CHEMBL ID	Drug name	HYAL2 XP score (kcal/mol)	Ligand efficiency	Interaction profiles	Type
				(3.01 Å), Glu68 (2.66 Å); π–π stacked: Tyr79 (4.05 Å)	
CHEMBL1200647	CANDICIDIN	-7.644	0.097	Conventional H-bond: Glu68 (3.26 Å), Lys118 (2.59 Å), Trp145 (3.00 Å); π–π stacked: Trp145 (5.01 Å); π-alkyl: Tyr253 (5.02 Å)	Dual
CHEMBL58	MITOXANTRONE	-8.046	0.259	Conventional H-bond: Asn67 (3.07 Å), Tyr79 (2.37 Å), Asp133 (2.37 Å); Salt bridge: Glu68 (2.71 Å); π–π stacked: Pro66 (5.49 Å)	Dual

The ligands CHEMBL1200647 (Candicidin) and CHEMBL58 (Mitoxantrone) exhibited dual binding (HYAL1: -10.4 and -8.3 kcal/mol; HYAL2: -7.7 and -8.1 kcal/mol, respectively). The interaction was stabilized by stacking between Tyr202/Tyr206 and Trp321/Trp325, along with strong hydrogen-bond interactions with conserved catalytic amino acids (Asp129/Glu131 in HYAL1; Asp133/Glu135 in HYAL2).

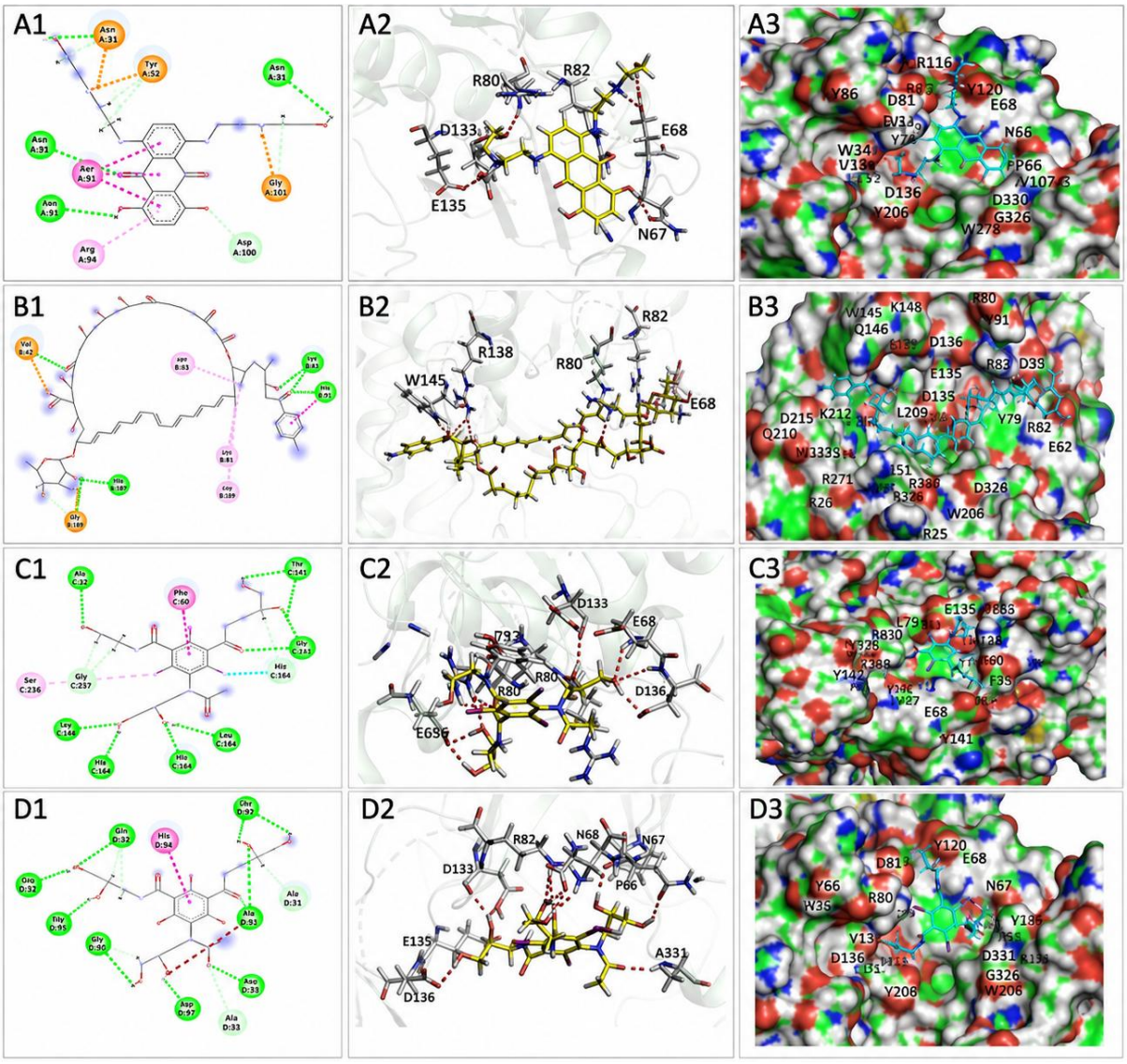

Figure 10. Molecular docking interactions of HYAL2 with FDA-approved ligands. (A) Mitoxantrone (CHEMBL58) and (B) Candicidin (CHEMBL1200647) show binding to conserved catalytic residues of HYAL2. (C) Ioxilan (CHEMBL1201075) and (D) Iohexol (CHEMBL1200455) represent HYAL2-selective ligands and exhibit isoform-specific interactions with the protein.

The observed interactions with key catalytic residues indicate that the dual-binding compounds may disrupt the enzymatic hydrolysis of hyaluronan in both isoforms, highlighting their potential as dual hyaluronidase inhibitors [35]. The binding orientations and key amino acid interactions of the top-scoring ligands are illustrated in Figure 9 (HYAL1) and Figure 10 (HYAL2), showing hydrogen-bonding and π–stacking interactions with the conserved catalytic residues of each isoform.

To provide a comparative benchmark, the known hyaluronidase inhibitor glycyrrhizin was docked into the HYAL1 catalytic pocket using the same Glide XP protocol. Glycyrrhizin exhibited a docking score of −6.379 kcal/mol, forming multiple hydrogen-bond interactions with key residues including Arg134, Glu131, Thr143, and Lys144, along with hydrophobic interactions involving Tyr75 and Trp321. These interactions are located within the catalytic binding cleft of HYAL1 and were used as a reference for evaluating the binding potential of the screened FDA-approved compounds. Among HYAL1-selective ligands, top hits included CHEMBL1200507 (Iodixanol, -10.8 kcal/mol) and CHEMBL1095607 (Reproterol, -9.7 kcal/mol). These docking scores indicate favorable predicted binding interactions within the catalytic pocket**,** although docking results represent computational predictions that require further experimental validation. Other HYAL1-selective compounds were CHEMBL2104771 (Reproterol hydrochloride, -9.7 kcal/mol) and CHEMBL1200555 (Iotrolan, -8.7 kcal/mol). These ligands formed hydrogen bonds with the catalytic dyad (Asp129, Glu131) and engaged in aromatic stacking with Tyr202 and Tyr247, key residues for substrate binding in HYAL1. Their larger scores than those of HYAL2 indicate isoform specificity and are similar to what has been reported for the role of HYAL1 in invasiveness and poor outcome of tumorous diseases [58,59]. It is likely that specific inhibitors of HYAL1 might be valuable for treating malignancies.

In contrast, several ligands showed high affinity for HYAL2. The optimal HYAL2-selective compounds were CHEMBL1200455 (Iohexol, -9.4 kcal/mol), CHEMBL1201075 (Ioxilan, -8.9 kcal/mol), CHEMBL1201202 (Fondaparinux, -8.7 kcal/mol), CHEMBL1200614 (Ioversol, -8.4 kcal/mol), and CHEMBL2364623 ((Plazomicin sulfate) -7.9 kcal/mol). All those ligands interacted unvaryingly with Glu135 and Asp133, as well as Arg138 and Tyr251, which are more predominant in HYAL2 than in HYAL1. These binding modes indicate that the development of HYAL2-specific inhibitors is feasible. Because HYAL2 acts at the plasma membrane to initiate extracellular HA cleavage [60], specific inhibition may be used.

Comparative analysis thus revealed distinct isoform selectivity. Dual binders targeted conserved catalytic residues across both isoforms, while selective ligands exploited isoform-dependent structural differences. This agrees with previous observations that HYAL1 and HYAL2 share catalytic mechanisms but differ in substrate specificity [35]. Biologically, dual inhibitors could provide broad-spectrum suppression of hyaluronidase activity in cancers with high HA turnover, while isoform-selective inhibitors could enable tailored potential therapeutic strategies.

3.10. Discussion.

The tumor microenvironment is an intricate biological system in which the host immune system and cancer cells continuously interact. Hyaluronan accumulates abnormally in tumors and contributes to tumor development. As HA-degrading enzymes, HAases may inhibit tumor growth [61]. Tumor cells can disrupt the normal balance of chemokines and inflammatory cytokines, thereby contributing to tumor development [62]. This pan-cancer

analysis highlights the roles of HYAL1 and HYAL2 in tumor development, progression, and immune modulation. They are the most essential mammalian hyaluronidases in somatic tissues. They may work together to reduce high molecular weight HA, a negatively charged glycosaminoglycan, to the tetrasaccharide level. HYAL2 hydrolyzes high molecular weight HA to generate an intermediate-sized product, which HYAL1 then hydrolyzes to yield small oligosaccharides [63]. Hyaluronan is thought to be involved in tumor invasion and metastatic dissemination. The presence of HA around tumor cells is often associated with cancer aggressiveness and poor prognosis [20,64]. Both genes encode hyaluronidases that degrade HA, a key component of the ECM [65], which is involved in cell proliferation, migration, and immune regulation. Deregulation of HA metabolism is increasingly linked to oncogenesis and TME remodeling, influencing cancer aggressiveness and therapeutic resistance [23,24,32].

During a pan-cancer benchmarking study, HYAL1 and HYAL2 were compared with conventional ECM-remodeling genes (MMPs, HAS1-3, and CD44) to contextualize their potential as biomarkers. Extensive TCGA pan-cancer studies consistently reveal that various MMPs (e.g., MMP1/9/11/13/14) are generally increased across cancers and frequently provide significant diagnostic separation, with more variable but at times cancer-specific predictive relevance, increasing the bar for ECM markers [66]. In contrast, the HA-synthesis arm (HAS1-3) exhibits cancer-type-dependent interactions with outcome, particularly HAS2, which is commonly enhanced. It relates to CAF/immune infiltration and predicts a poor prognosis in some malignancies, indicating the pathway-level impact of hyaluronan turnover [67]. Recent pan-cancer analyses combining bulk and single-cell data for CD44, the principal HA receptor, have demonstrated strong associations with tumor stage, immune infiltration (including macrophage polarization), and survival. They have also shown predictive value for immunotherapy response, highlighting CD44's robust prognostic signal across cancers [68]. HYAL1 is frequently used as an individualized prognosticator in genitourinary tumors (prostate and bladder). In contrast, stromal HYAL2 in breast cancer correlates with tumor size, nodal status, and poor disease-free survival, implying that HA-degradation status adds non-redundant information to synthesis and receptor markers [69–71].

Several underlying mechanisms may be driving the tissue-specific differences in HYAL gene expression. According to previous studies, one possibility is epigenetic regulation; promoter hypermethylation can silence HYAL genes in certain cancer types [72]. For example, the downregulation of HYAL1 in bladder cancer could result from epigenetic silencing, given HYAL1's role as a tumor suppressor in bladder and prostate cancer [73]. Tumor molecular subtypes also seem to play a role: differences in expression levels across BRCA subtypes (e.g., BRCA-Her2 vs. BRCA-LumA) reflect the underlying transcriptional programs unique to each subtype. Moreover, the TME, particularly the ECM composition, can affect HYAL expression, given the enzymes' roles in degrading HA, which is abundant in some tumors (e.g., pancreatic and prostate cancers). This process may facilitate tumor invasion and metastasis. The oncogenic signaling pathways, including TGF-β, PI3K/AKT, and Wnt, may regulate HYALs transcriptionally, further contributing to their varied expression profiles [74]. These enzymes may collaborate to break down high-molecular-weight hyaluronan (HA, a negatively charged, high-molecular-weight glycosaminoglycan) to the tetrasaccharide level [63,64].

Our research showed that HYAL1 and HYAL2 are detected differently in various tumors. There is significant overexpression in cancers like bladder, lung, and kidney cancers, but downregulation in others, such as colorectal and breast cancers. These patterns suggest tissue-specific functions and support earlier findings that HYAL1 promotes tumor invasion and

metastasis by degrading the extracellular matrix and angiogenesis [74]. On the other hand, some studies suggest that HYAL1 has tumor-suppressive roles in specific micro-environmental contexts, highlighting its dual functionality depending on the cell type and tumor [24]. Our clinical outcome analyses use KM survival curves to show a strong relationship between HYAL1/HYAL2 expression and patient survival. For example, high HYAL1 expression was tied to poor survival in bladder cancer and lung adenocarcinoma, but it showed a protective effect in kidney cancer and renal cell carcinoma. Similarly, HYAL2 expression was linked to shorter survival in mesothelioma and low-grade glioma, but it indicated better outcomes in uveal melanoma and kidney cancer. HYAL2 expression in myeloid cells associated with tumors drives inflammation in bladder cancer, helping the cancer evade the immune system and progress [27].

Our proteomic analysis, based on CPTAC data, supported the transcriptomic findings. It showed a significant increase in HYAL1 and HYAL2 protein levels in several cancers, including LUAD, HNSC, and KIRC. This suggests that HYAL enzymes play an active role in remodeling the TME, facilitating the spread of cancer cells and influencing the movement of immune cells. Although both genes had low rates of somatic mutations, our results highlighted some notable hotspots, such as HYAL1 A311V and HYAL2 R234S, that need further investigation for potential effects. These findings align with data from other pan-cancer studies, which show that low-frequency mutations that affect function contribute to tumor heterogeneity and progression. Our promoter methylation analysis also revealed significant epigenetic changes in HYAL1 and HYAL2 across various cancer types [26]. This suggests that methylation is key in regulating their expression, especially in BRCA, KIRC, and HNSC. Previous studies have shown that hypermethylation of tumor suppressor genes or hypomethylation of oncogenes is a common mechanism in cancer development, supporting our findings. Notably, our analysis of immune cell infiltration revealed that the expression of HYAL1 and HYAL2 correlates with CD8+ T cell infiltration in a cancer-type-specific manner. This suggests a potential role in immune surveillance and escape. For example, HYAL2 showed strong positive correlations with CD8+ T cell infiltration in BRCA-Basal and ESCA. This may reflect enhanced antigen presentation or chemotactic signaling. We found that high HYAL2 expression in renal cancer is linked with immunosuppressive myeloid-derived suppressor cells and PD-L1+ immune clusters. These interactions highlight HYAL1 and HYAL2 as key modulators of the tumor microenvironment, underscoring their potential as targets for immunotherapeutic intervention [45].

Docking studies with FDA-approved ligands and HYAL1 versus HYAL2 revealed isoform selectivity. As illustrated in Figures 9 and 10, the docking interactions clearly show the differential binding orientations and residue-level interactions of HYAL1- and HYAL2-selective ligands, supporting the observed isoform-specific binding patterns discussed above. Some compounds, such as CHEMBL1200647 and CHEMBL58, demonstrated favorable docking orientations within the catalytic pockets of both enzymes**,** suggesting their potential as candidate binders. Some compounds, such as CHEMBL1200647 and CHEMBL58, showed significant inhibitory activity against two enzymes, suggesting dual inhibitors of hyaluronidase discriminators. They targeted conserved catalytic residues (Asp129/Glu131 for HYAL1 and Asp133/Glu135 for HYAL2). In contrast, the ligands CHEMBL1200507 and CHEMBL1095607 exhibited selective HYAL1 binding with extra stabilizing interactions with Tyr202 and Tyr247. Because HYAL1 is frequently overexpressed in invasive tumors, these ligands may emerge as potential therapeutics for HYAL1-driven cancers. On the other hand,

ligands including CHEMBL1200455 and CHEMBL1201075 were HYAL2-selective and showed strong hydrogen bonds towards Glu135 and Arg138. As HYAL2 acts preferentially at the cell surface during ECM degradation, its selective blockade may help control tumor growth by altering the extracellular environment. It should be noted that docking scores provide only an approximation of ligand-protein interactions and do not represent experimentally determined binding affinities. Therefore, further studies such as molecular dynamics simulations, free-energy calculations, and biochemical assays will be necessary to confirm the predicted interactions.

Taken together, these data underscore HYAL1 and HYAL2 as context-dependent biomarkers with far-reaching prognostic and immunological implications. Expression signatures, methylation profiles, and immune infiltration levels, when integrated into predictive models, might help stratify patients more accurately and predict therapy needs. Significantly, the docking results indicate that broad-spectrum inhibitors targeting multiple isoforms, as well as isoform-specific drugs, could be developed for personalized treatments. However, additional functional applications based on in vitro studies and clinical trials will be needed to validate the pharmacological roles of these candidate ligands and to assess the possible roles of HYAL1 and HYAL2 in tumorigenesis.

4. Conclusions

This pan-cancer analysis describes the multifunctional roles of HYAL1 and HYAL2 in human cancers. HYAL1 and HYAL2 are the primary hyaluronidases in human cells that regulate intercellular interactions with the tumor microenvironment, providing significant targets for cancer therapy. HYAL1 and HYAL2 exhibit cancer-specific differential expression, significant epigenetic regulation via promoter methylation, and strong correlations with overall survival and CD8+ T cell infiltration across 33 tumor types. However, low mutation frequencies and the consistent associations of HYAL1 and HYAL2 with prognostic outcomes and immune modulation highlight their potential as cell-specific biomarkers in targeted cancer therapy. These findings demonstrate that HYAL1 and HYAL2 could be potential predictive biomarkers that influence the tumor immune environment and provide insights for precision oncology and immunotherapy. To extend these findings, molecular docking with FDA-approved drugs against HYAL1 (PDB: 2PE4) and HYAL2 (AlphaFold) revealed high-affinity ligands, including HYAL1-selective (CHEMBL1200507), HYAL2-selective (CHEMBL1200455), and dual inhibitors (CHEMBL58, CHEMBL1200647). These findings suggest that drug repurposing may provide potential candidate compounds targeting hyaluronidase activity, although further computational and experimental validation will be required to confirm their inhibitory activity.

5. Limitations and Future Recommendations

This study relies heavily on bioinformatics analyses of publicly available datasets, which may introduce biases and lack specific clinical details. The findings are only correlational and have not been validated through experimental or clinical studies, which limits our understanding of the underlying biological mechanisms. The analysis did not account for tumor heterogeneity or cell-type-specific effects, as it only used bulk RNA sequencing data. This study focuses only on the HYAL1 and HYAL2 genes because of their established roles in HA metabolism and cancer progression. We have excluded the other 3p21.3 genes, like

RASSF1A and FUS1, for lack of available data. Additionally, transcriptomic data may not always accurately reflect protein activity or functional enzymatic levels. Tumor heterogeneity and differences in clinical annotations across datasets may also influence the observed associations. Further in vitro and in vivo studies are needed to confirm the functional roles of HYAL1 and HYAL2 in cancer progression and immune regulation.

Author Contributions

Conceptualization, M.N.U. and N.K.S.; methodology, N.K.S. and M.S.M.; software, M.N.U. and N.K.S.; validation, R.M. and M.N.U.; formal analysis, N.K.S. and M.S.M.; investigation, M.N.U. and R.M.; resources, M.N.U. and N.K.S.; data curation, N.K.S. and M.S.M.; writing—original draft preparation, N.K.S. and M.S.M.; writing—review and editing, R.M. and M.N.U.; visualization, N.K.S. and M.S.M.; supervision, M.N.U.; project administration, M.N.U. All authors have read and agreed to the published version of the manuscript.

Institutional Review Board Statement

Not applicable.

Informed Consent Statement

Not applicable.

Data Availability Statement

Data supporting the findings of this study are available upon reasonable request from the corresponding author.

Funding

This research received no external funding.

Acknowledgments

The authors would like to thank the Institute of Food Science and Technology, Bangladesh Council of Scientific and Industrial Research, Dhaka, 1205, Bangladesh.

Conflicts of Interest

The author declares no conflicts of interest.

Abbreviations

The following abbreviations are used in this manuscript:

Abbreviation	Definition
TCGA	The Cancer Genome Atlas
ECM	Extracellular Matrix
MDSCs	Myeloid-Derived Suppressor Cells
TAMs	Tumor-Associated Macrophages
CAFs	Cancer-Associated Fibroblasts
VUS	Variants of Uncertain Significance
KM	Kaplan-Meier
HR	Hazard Ratio

Abbreviation	Definition
TME	Tumor Microenvironment
HA	Hyaluronic Acid
IVD	Intervertebral Disc
CPTAC	Clinical Proteomic Tumor Analysis Consortium
OS	Overall Survival
FDR	False Discovery Rate
RNA	Ribonucleic Acid
PDB	Protein Data Bank
FDA	Food and Drug Administration
HYAL1	Hyaluronidase 1
HYAL2	Hyaluronidase 2

References

1. Wéber, A.; Vignat, J.; Shah, R.; Morgan, E.; Laversanne, M.; Nagy, P.; Kenessey, I.; Znaor, A. Global burden of bladder cancer mortality in 2020 and 2040 according to GLOBOCAN estimates. *World J. Urol.* **2024**, *42*, 237, https://doi.org/10.1007/s00345-024-04949-8.
2. Chao, K.L.; Muthukumar, L.; Herzberg, O. Structure of Human Hyaluronidase-1, a Hyaluronan Hydrolyzing Enzyme Involved in Tumor Growth and Angiogenesis. *Biochemistry* **2007**, *46*, 6911-6920, https://doi.org/10.1021/bi700382g.
3. Liu, Y.; Wang, D.; Li, Z.; Li, X.; Jin, M.; Jia, N.; Cui, X.; Hu, G.; Tang, T.; Yu, Q. Pan-cancer analysis on the role of PIK3R1 and PIK3R2 in human tumors. *Sci. Rep.* **2022**, *12*, 5924, https://doi.org/10.1038/s41598-022-09889-0.
4. Deng, M.; Brägelmann, J.; Schultze, J.L.; Perner, S. Web-TCGA: an online platform for integrated analysis of molecular cancer data sets. *BMC Bioinformatics* **2016**, *17*, 72, https://doi.org/10.1186/s12859-016-0917-9.
5. Tomczak, K.; Czerwińska, P.; Wiznerowicz, M. Review The Cancer Genome Atlas (TCGA): an immeasurable source of knowledge. *Contemp. Oncol.* **2015**, *19*, A68-A77, https://doi.org/10.5114/wo.2014.47136.
6. Hu, Q.; Zhu, Y.; Mei, J.; Liu, Y.; Zhou, G. Extracellular matrix dynamics in tumor immunoregulation: from tumor microenvironment to immunotherapy. *J. Hematol. Oncol.* **2025**, *18*, 65, https://doi.org/10.1186/s13045-025-01717-y.
7. Fink, S.P.; Triggs-Raine, B. Genetic Deficiencies of Hyaluronan Degradation. *Cells* **2024**, *13*, 1203, https://doi.org/10.3390/cells13141203.
8. Stern, R. CHAPTER 12 - Hyaluronidases in Cancer Biology. In Hyaluronan in Cancer Biology, Stern, R., Ed.; Academic Press: San Diego, **2008**; pp. 207-220, https://doi.org/10.1016/B978-012374178-3.10012-2.
9. Gong, P.; Wang, F.; Hua, Y.; Ying, J.; Chen, J.; Qiao, Y. Collagenase-mediated extracellular matrix targeting for enhanced drug penetration and therapeutic efficacy in nanoscale delivery systems for cancer therapy. *J. Nanobiotechnology* **2025**, *23*, 733, https://doi.org/10.1186/s12951-025-03815-y.
10. Zhou, F.; Mu, G.; Bi, H.; Chen, L.; Zha, Z.; Jin, Y.; Chiu, M.L. Targeted Hyaluronan Degradation Enhanced Tumor Growth Inhibition in Gastrointestinal Cancer Models. *Cancers* **2025**, *17*, 3411, https://doi.org/10.3390/cancers17213411.
11. Bourguignon, L.Y.W.; Shiina, M.; Li, J.-J. Chapter Ten - Hyaluronan–CD44 Interaction Promotes Oncogenic Signaling, microRNA Functions, Chemoresistance, and Radiation Resistance in Cancer Stem Cells Leading to Tumor Progression. In Advances in Cancer Research, Simpson, M.A., Heldin, P., Eds.; Academic Press: **2014**; Volume 123, pp. 255-275, https://doi.org/10.1016/b978-0-12-800092-2.00010-1.
12. Fujisawa, S.; Takagi, K.; Yamaguchi-Tanaka, M.; Sato, A.; Miki, Y.; Miyashita, M.; Tada, H.; Ishida, T.; Suzuki, T. Clinicopathological significance of hyaluronan and hyaluronidase 2 (HYAL2) in breast cancer. *Pathol. Res. Pract.* **2024**, *260*, 155434, https://doi.org/10.1016/j.prp.2024.155434.
13. Bouga, H.; Tsouros, I.; Bounias, D.; Kyriakopoulou, D.; Stavropoulos, M.S.; Papageorgakopoulou, N.; Vynios, D.H. Involvement of hyaluronidases in colorectal cancer. *BMC cancer*. **2010**, *10*, 499. https://doi.org/10.1186/1471-2407-10-499.
14. Yuan, J.; Hou, B.; Guo, K.; Zhu, J.; Xiao, H. Tumor-derived exosomal hyaluronidase 1 induced M2 macrophage polarization and promoted esophageal cancer progression. *Exp. Cell Res.* **2024**, *439*, 113963, https://doi.org/10.1016/j.yexcr.2024.113963.

15. Yin, Q.; Yang, X.; Li, L.; Xu, T.; Zhou, W.; Gu, W.; Ma, F.; Yang, R. The Association Between Breast Cancer and Blood-Based Methylation of *S100P* and *HYAL2* in the Chinese Population. *Front. Genet.* **2020**, *11*, 977, https://doi.org/10.3389/fgene.2020.00977.
16. Yifei, Y.I.N.; Hong, L.I.; Chunsheng, Y.; Mengxia, L.I.; Rongxi, Y. Detection of DNA methylation of HYAL2 gene for differentiating malignant from benign thyroid tumors. *J. South. Med. Univ.* **2022**, *42*, 123-129, https://doi.org/10.12122/j.issn.1673-4254.2022.01.15.
17. Kumar, K.; Kanojia, D.; Bentrem, D.J.; Hwang, R.F.; Butchar, J.P.; Tridandapani, S.; Munshi, H.G. Targeting BET Proteins Decreases Hyaluronidase-1 in Pancreatic Cancer. *Cells* **2023**, *12*, 1490, https://doi.org/10.3390/cells12111490.
18. Ruppert, S.M.; Hawn, T.R.; Arrigoni, A.; Wight, T.N.; Bollyky, P.L. Tissue integrity signals communicated by high-molecular weight hyaluronan and the resolution of inflammation. *Immunol. Res.* **2014**, *58*, 186-192, https://doi.org/10.1007/s12026-014-8495-2.
19. Liu, Y.; Zhang, Z.; Xia, Y.; Ran, M.; Wang, Q.; Wu, Q.; Yu, W.; Li, C.; Li, S.; Guo, N. Dual-targeting of tumor cells and tumor-associated macrophages by hyaluronic acid-modified MnO_2 for enhanced sonodynamic therapy. *Int. J. Biol. Macromol.* **2024**, *283*, 137543, https://doi.org/10.1016/j.ijbiomac.2024.137543.
20. Wang, F.; Grigorieva, E.V.; Li, J.; Senchenko, V.N.; Pavlova, T.V.; Anedchenko, E.A.; Kudryavtseva, A.V.; Tsimanis, A.; Angeloni, D.; Lerman, M.I.; Kashuba, V.I.; Klein, G.; Zabarovsky, E.R. *HYAL1* and *HYAL2* Inhibit Tumour Growth *In Vivo* but Not *In Vitro*. *PLOS ONE* **2008**, *3*, e3031, https://doi.org/10.1371/journal.pone.0003031.
21. Lu, J.; Zhao, Z.; Pan, L.; Wu, H.; Wang, S.; Tong, X.; Wu, S. Hyaluronidase: structure, mechanism of action, diseases and therapeutic targets. *Mol. Biomed.* **2025**, *6*, 50, https://doi.org/10.1186/s43556-025-00299-y.
22. Schmaus, A.; Spataro, S.; Sallmann, P.; Möller, S.; Scapozza, L.; Prunotto, M.; Sleeman, J.P. A Novel, Cell-Compatible Hyaluronidase Activity Assay Identifies Dextran Sulfates and Other Sulfated Polymeric Hydrocarbons as Potent Inhibitors for CEMIP. *Cells* **2025**, *14*, 101, https://doi.org/10.3390/cells14020101.
23. Chanmee, T.; Ontong, P.; Itano, N. Hyaluronan: A modulator of the tumor microenvironment. *Cancer Lett.* **2016**, *375*, 20-30, https://doi.org/10.1016/j.canlet.2016.02.031.
24. Harada, H.; Takahashi, M. CD44-dependent Intracellular and Extracellular Catabolism of Hyaluronic Acid by Hyaluronidase-1 and -2*. *J. Biol. Chem.* **2007**, *282*, 5597-5607, https://doi.org/10.1074/jbc.M608358200.
25. Donelan, W.; Dominguez-Gutierrez, P.R.; Kusmartsev, S. Deregulated hyaluronan metabolism in the tumor microenvironment drives cancer inflammation and tumor-associated immune suppression. *Front. Immunol.* **2022**, *13*, 971278, https://doi.org/10.3389/fimmu.2022.971278.
26. Kusmartsev, S.; Kwenda, E.; Dominguez-Gutierrez, P.R.; Crispen, P.L.; O'Malley, P. High Levels of PD-L1+ and Hyal2+ Myeloid-derived Suppressor Cells in Renal Cell Carcinoma. *J. Kidney Cancer* **2022**, *9*, 1–6, https://doi.org/10.15586/jkcvhl.v9i2.208.
27. Dominguez-Gutierrez, P.R.; Kwenda, E.P.; Donelan, W.; O'Malley, P.; Crispen, P.L.; Kusmartsev, S. Hyal2 Expression in Tumor-Associated Myeloid Cells Mediates Cancer-Related Inflammation in Bladder Cancer. *Cancer Res.* **2021**, *81*, 648-657, https://doi.org/10.1158/0008-5472.CAN-20-1144.
28. Puissant, E.; Boonen, M. Monocytes/Macrophages Upregulate the Hyaluronidase HYAL1 and Adapt Its Subcellular Trafficking to Promote Extracellular Residency upon Differentiation into Osteoclasts. *PLOS ONE* **2016**, *11*, e0165004, https://doi.org/10.1371/journal.pone.0165004.
29. Karousou, E.; Parnigoni, A.; Moretto, P.; Passi, A.; Viola, M.; Vigetti, D. Hyaluronan in the cancer cells microenvironment. *Cancers*. **2023,** *15*, 798. https://doi.org/10.3390/cancers15030798.
30. Karamanos, N.K.; Theocharis, A.D.; Piperigkou, Z.; Manou, D.; Passi, A.; Skandalis, S.S.; Vynios, D.H.; Orian-Rousseau, V.; Ricard-Blum, S.; Schmelzer, C.E.H.; Duca, L.; Durbeej, M.; Afratis, N.A.; Troeberg, L.; Franchi, M.; Masola, V.; Onisto, M. A guide to the composition and functions of the extracellular matrix. *FEBS J.* **2021**, *288*, 6850-6912, https://doi.org/10.1111/febs.15776.
31. Litwiniuk, M.; Krejner, A.; Speyrer, M.S.; Gauto, A.R.; Grzela, T. Hyaluronic Acid in Inflammation and Tissue Regeneration. *Wounds* **2016**, *28*, 78-88.
32. Dominguez-Gutierrez, P.R.; Kwenda, E.P.; Donelan, W.; Miranda, M.; Doty, A.; O'Malley, P.; Crispen, P.L.; Kusmartsev, S. Detection of PD-L1–Expressing Myeloid Cell Clusters in the Hyaluronan-Enriched Stroma in Tumor Tissue and Tumor-Draining Lymph Nodes. *J. Immunol.* **2022**, *208*, 2829-2836, https://doi.org/10.4049/jimmunol.2100026.

33. Clough, E.; Barrett, T. The Gene Expression Omnibus Database. In Statistical Genomics: Methods and Protocols, Mathé, E., Davis, S., Eds.; Springer New York: New York, NY, **2016**; pp. 93-110, https://doi.org/10.1007/978-1-4939-3578-9_5.
34. Blum, A.; Wang, P.; Zenklusen, J.C. SnapShot: TCGA-Analyzed Tumors. *Cell* **2018**, *173*, 530, https://doi.org/10.1016/j.cell.2018.03.059.
35. Jumper, J.; Evans, R.; Pritzel, A.; Green, T.; Figurnov, M.; Ronneberger, O.; Tunyasuvunakool, K.; Bates, R.; Žídek, A.; Potapenko, A.; Bridgland, A.; Meyer, C.; Kohl, S.A.A.; Ballard, A.J.; Cowie, A.; Romera-Paredes, B.; Nikolov, S.; Jain, R.; Adler, J.; Back, T.; Petersen, S.; Reiman, D.; Clancy, E.; Zielinski, M.; Steinegger, M.; Pacholska, M.; Berghammer, T.; Bodenstein, S.; Silver, D.; Vinyals, O.; Senior, A.W.; Kavukcuoglu, K.; Kohli, P.; Hassabis, D. Highly accurate protein structure prediction with AlphaFold. *Nature* **2021**, *596*, 583-589, https://doi.org/10.1038/s41586-021-03819-2.
36. Pushpakom, S.; Iorio, F.; Eyers, P.A.; Escott, K.J.; Hopper, S.; Wells, A.; Doig, A.; Guilliams, T.; Latimer, J.; McNamee, C.; Norris, A.; Sanseau, P.; Cavalla, D.; Pirmohamed, M. Drug repurposing: progress, challenges and recommendations. *Nat. Rev. Drug Discov.* **2019**, *18*, 41-58, https://doi.org/10.1038/nrd.2018.168.
37. Friesner, R.A.; Banks, J.L.; Murphy, R.B.; Halgren, T.A.; Klicic, J.J.; Mainz, D.T.; Repasky, M.P.; Knoll, E.H.; Shelley, M.; Perry, J.K.; Shaw, D.E.; Francis, P.; Shenkin, P.S. Glide: A New Approach for Rapid, Accurate Docking and Scoring. 1. Method and Assessment of Docking Accuracy. *J. Med. Chem.* **2004**, *47*, 1739-1749, https://doi.org/10.1021/jm0306430.
38. Halgren, T.A.; Murphy, R.B.; Friesner, R.A.; Beard, H.S.; Frye, L.L.; Pollard, W.T.; Banks, J.L. Glide: A New Approach for Rapid, Accurate Docking and Scoring. 2. Enrichment Factors in Database Screening. *J. Med. Chem.* **2004**, *47*, 1750-1759, https://doi.org/10.1021/jm030644s.
39. Murphy, R.B.; Repasky, M.P.; Greenwood, J.R.; Tubert-Brohman, I.; Jerome, S.; Annabhimoju, R.; Boyles, N.A.; Schmitz, C.D.; Abel, R.; Farid, R.; Friesner, R.A. WScore: A Flexible and Accurate Treatment of Explicit Water Molecules in Ligand–Receptor Docking. *J. Med. Chem.* **2016**, *59*, 4364-4384, https://doi.org/10.1021/acs.jmedchem.6b00131.
40. Li, T.; Fu, J.; Zeng, Z.; Cohen, D.; Li, J.; Chen, Q.; Li, B.; Liu, X.S. TIMER2.0 for analysis of tumor-infiltrating immune cells. *Nucleic Acids Res.* **2020**, *48*, W509-W514, https://doi.org/10.1093/nar/gkaa407.
41. Tang, Z.; Kang, B.; Li, C.; Chen, T.; Zhang, Z. GEPIA2: an enhanced web server for large-scale expression profiling and interactive analysis. *Nucleic Acids Res.* **2019**, *47*, W556-W560, https://doi.org/10.1093/nar/gkz430.
42. Chandrashekar, D.S.; Bashel, B.; Balasubramanya, S.A.H.; Creighton, C.J.; Ponce-Rodriguez, I.; Chakravarthi, B.V.S.K.; Varambally, S. UALCAN: A Portal for Facilitating Tumor Subgroup Gene Expression and Survival Analyses. *Neoplasia* **2017**, *19*, 649-658, https://doi.org/10.1016/j.neo.2017.05.002.
43. Chandrashekar, D.S.; Karthikeyan, S.K.; Korla, P.K.; Patel, H.; Shovon, A.R.; Athar, M.; Netto, G.J.; Qin, Z.S.; Kumar, S.; Manne, U.; Creighton, C.J.; Varambally, S. UALCAN: An update to the integrated cancer data analysis platform. *Neoplasia* **2022**, *25*, 18-27, https://doi.org/10.1016/j.neo.2022.01.001.
44. Chen, J.; Mai, H.; Chen, H.; Zhou, B.; Hou, J.; Jiang, D.-K. Pan-Cancer Analysis Identified *C1ORF112* as a Potential Biomarker for Multiple Tumor Types. *Front. Mol. Biosci.* **2021**, *8*, 693651, https://doi.org/10.3389/fmolb.2021.693651.
45. Yang, X.; Gao, L.; Zhang, S. Comparative pan-cancer DNA methylation analysis reveals cancer common and specific patterns. *Brief. Bioinform.* **2017**, *18*, 761-773, https://doi.org/10.1093/bib/bbw063.
46. Győrffy, B.; Lanczky, A.; Eklund, A.C.; Denkert, C.; Budczies, J.; Li, Q.; Szallasi, Z. An online survival analysis tool to rapidly assess the effect of 22,277 genes on breast cancer prognosis using microarray data of 1,809 patients. *Breast Cancer Res. Treat.* **2010**, *123*, 725-731, https://doi.org/10.1007/s10549-009-0674-9.
47. Győrffy, B. Integrated analysis of public datasets for the discovery and validation of survival-associated genes in solid tumors. *Innovation* **2024**, *5*, 100625, https://doi.org/10.1016/j.xinn.2024.100625.
48. Ahmed, M.Z.; Billah, M.M.; Ferdous, J.; Antar, S.I.; Al Mamun, A.; Hossain, M.J. Pan-cancer analysis reveals immunological and prognostic significance of CCT5 in human tumors. *Sci. Rep.* **2025**, *15*, 14405, https://doi.org/10.1038/s41598-025-88339-z.
49. Huang, Y.; Wu, L.; Sun, Y.; Li, J.; Mao, N.; Yang, Y.; Zhao, M.; Ren, S. CCL5 might be a prognostic biomarker and associated with immuno-therapeutic efficacy in cancers: A pan-cancer analysis. *Heliyon* **2023**, *9*, e18215, https://doi.org/10.1016/j.heliyon.2023.e18215.
50. AlphaFold Protein Structure Database Available online: https://alphafold.com/entry/Q9Z2Q3 (accessed on 26 September **2025**).

51. Harder, E.; Damm, W.; Maple, J.; Wu, C.; Reboul, M.; Xiang, J.Y.; Wang, L.; Lupyan, D.; Dahlgren, M.K.; Knight, J.L.; Kaus, J.W.; Cerutti, D.S.; Krilov, G.; Jorgensen, W.L.; Abel, R.; Friesner, R.A. OPLS3: A Force Field Providing Broad Coverage of Drug-like Small Molecules and Proteins. *J. Chem. Theory Comput.* **2016**, *12*, 281-296, https://doi.org/10.1021/acs.jctc.5b00864.
52. Madhavi Sastry, G.; Adzhigirey, M.; Day, T.; Annabhimoju, R.; Sherman, W. Protein and ligand preparation: parameters, protocols, and influence on virtual screening enrichments. *J. Comput. Aided Mol. Des.* **2013**, *27*, 221-234, https://doi.org/10.1007/s10822-013-9644-8.
53. Roos, K.; Wu, C.; Damm, W.; Reboul, M.; Stevenson, J.M.; Lu, C.; Harder, E.D. OPLS3e: Extending force field coverage for drug-like small molecules. *J. chem. theor. comput.* 2019, *15*, 1863-1874. https://doi.org/10.1021/acs.jctc.8b01026.
54. Zhang, L.; Bharadwaj, A.G.; Casper, A.; Barkley, J.; Barycki, J.J.; Simpson, M.A. Hyaluronidase Activity of Human Hyal1 Requires Active Site Acidic and Tyrosine Residues*. *J. Biol. Chem.* **2009**, *284*, 9433-9442, https://doi.org/10.1074/jbc.M900210200.
55. Kozakov, D.; Grove, L.E.; Hall, D.R.; Bohnuud, T.; Mottarella, S.E.; Luo, L.; Xia, B.; Beglov, D.; Vajda, S. The FTMap family of web servers for determining and characterizing ligand-binding hot spots of proteins. *Nat. Protoc.* **2015**, *10*, 733-755, https://doi.org/10.1038/nprot.2015.043.
56. Omar, A.M.; Aljahdali, A.S.; Safo, M.K.; Mohamed, G.A.; Ibrahim, S.R.M. Docking and Molecular Dynamic Investigations of Phenylspirodrimanes as Cannabinoid Receptor-2 Agonists. *Molecules* **2023**, *28*, 44, https://doi.org/10.3390/molecules28010044.
57. Friesner, R.A.; Murphy, R.B.; Repasky, M.P.; Frye, L.L.; Greenwood, J.R.; Halgren, T.A.; Sanschagrin, P.C.; Mainz, D.T. Extra Precision Glide: Docking and Scoring Incorporating a Model of Hydrophobic Enclosure for Protein−Ligand Complexes. *J. Med. Chem.* **2006**, *49*, 6177-6196, https://doi.org/10.1021/jm051256o.
58. Kultti, A.; Li, X.; Jiang, P.; Thompson, C.B.; Frost, G.I.; Shepard, H.M. Therapeutic Targeting of Hyaluronan in the Tumor Stroma. *Cancers* **2012**, *4*, 873-903, https://doi.org/10.3390/cancers4030873.
59. McAtee, C.O.; Barycki, J.J.; Simpson, M.A. Emerging roles for hyaluronidase in cancer metastasis and therapy. *Adv. Cancer Res.* **2014**, *123*, 1-34. https://doi.org/10.1016/B978-0-12-800092-2.00001-0.
60. Yamaguchi, Y. TMEM2: A New Dimension in Hyaluronan Biology. *Proteoglycan Research*, **2025**, 3, e70021. https://doi.org/10.1002/pgr2.70021.
61. Jin, Z.; Zhang, G.; Liu, Y.; He, Y.; Yang, C.; Du, Y.; Gao, F. The suppressive role of HYAL1 and HYAL2 in the metastasis of colorectal cancer. *J. Gastroenterol. Hepatol.* **2019**, *34*, 1766-1776, https://doi.org/10.1111/jgh.14660.
62. Gentles, A.J.; Newman, A.M.; Liu, C.L.; Bratman, S.V.; Feng, W.; Kim, D.; Nair, V.S.; Xu, Y.; Khuong, A.; Hoang, C.D.; Diehn, M.; West, R.B.; Plevritis, S.K.; Alizadeh, A.A. The prognostic landscape of genes and infiltrating immune cells across human cancers. *Nat. Med.* **2015**, *21*, 938-945, https://doi.org/10.1038/nm.3909.
63. Csoka, A.B.; Frost, G.I.; Stern, R. The six hyaluronidase-like genes in the human and mouse genomes. *Matrix Biol.* **2001**, *20*, 499-508, https://doi.org/10.1016/S0945-053X(01)00172-X.
64. Cirillo, N. The Hyaluronan/CD44 Axis: A Double-Edged Sword in Cancer. *Int. J. Mol. Sci.* **2023**, *24*, 15812. https://doi.org/10.3390/ijms242115812.
65. Hautmann, S.H.; Lokeshwar, V.B.; Schroeder, G.L.; Civantos, F.; Duncan, R.C.; Gnann, R.; Friedrich, M.G.; Soloway, M.S. Elevated tissue expression of hyaluronic acid and hyaluronidase validates the HA-HAase urine test for bladder cancer. *J. Urol.* **2001**, *165*, 2068-2074, https://doi.org/10.1016/S0022-5347(05)66296-9.
66. Gobin, E.; Bagwell, K.; Wagner, J.; Mysona, D.; Sandirasegarane, S.; Smith, N.; Bai, S.; Sharma, A.; Schleifer, R.; She, J.-X. A pan-cancer perspective of matrix metalloproteases (MMP) gene expression profile and their diagnostic/prognostic potential. *BMC Cancer* **2019**, *19*, 581, https://doi.org/10.1186/s12885-019-5768-0.
67. Bao, X.; Ran, J.; Kong, C.; Wan, Z.; Wang, J.; Yu, T.; Ruan, S.; Ding, W.; Xia, L.; Zhang, D. Pan-cancer analysis reveals the potential of hyaluronate synthase as therapeutic targets in human tumors. *Heliyon* **2023**, *9*, e19112, https://doi.org/10.1016/j.heliyon.2023.e19112.
68. Zhang, Q.; Wang, X.; Liu, Y.; Xu, H.; Ye, C. Pan-cancer and single-cell analyses identify CD44 as an immunotherapy response predictor and regulating macrophage polarization and tumor progression in colorectal cancer. *Front. Oncol.* **2024**, *14*, 1380821, https://doi.org/10.3389/fonc.2024.1380821.
69. Morera, D.S.; Hennig, M.S.; Talukder, A.; Lokeshwar, S.D.; Wang, J.; Garcia-Roig, M.; Ortiz, N.; Yates, T.J.; Lopez, L.E.; Kallifatidis, G.; Kramer, M.W.; Jordan, A.R.; Merseburger, A.S.; Manoharan, M.; Soloway, M.S.; Terris, M.K.; Lokeshwar, V.B. Hyaluronic acid family in bladder cancer: potential prognostic

biomarkers and therapeutic targets. *Br. J. Cancer* **2017**, *117*, 1507-1517, https://doi.org/10.1038/bjc.2017.318.
70. Posey, J.T.; Soloway, M.S.; Ekici, S.; Sofer, M.; Civantos, F.; Duncan, R.C.; Lokeshwar, V.B. Evaluation of the prognostic potential of hyaluronic acid and hyaluronidase (HYAL1) for prostate cancer. *Cancer Res.* **2003**, *63*, 2638-2644.
71. Ekici, S.; Cerwinka, W.H.; Duncan, R.; Gomez, P.; Civantos, F.; Soloway, M.S.; Lokeshwar, V.B. Comparison of the prognostic potential of hyaluronic acid, hyaluronidase (HYAL-1), CD44v6 and microvessel density for prostate cancer. *Int. J. Cancer* **2004**, *112*, 121-129, https://doi.org/10.1002/ijc.20368.
72. Du, W.; Xia, X.; Hu, F.; Yu, J. Extracellular matrix remodeling in the tumor immunity. *Front. Immunol.* **2024**, *14*, 1340634, https://doi.org/10.3389/fimmu.2023.1340634.
73. Lokeshwar, V.B.; Rubinowicz, D.; Schroeder, G.L.; Forgacs, E.; Minna, J.D.; Block, N.L.; Nadji, M.; Lokeshwar, B.L. Stromal and Epithelial Expression of Tumor Markers Hyaluronic Acid and HYAL1 Hyaluronidase in Prostate Cancer*. *J. Biol. Chem.* **2001**, *276*, 11922-11932, https://doi.org/10.1074/jbc.M008432200.
74. Michalczyk, M.; Humeniuk, E.; Adamczuk, G.; Korga-Plewko, A. Hyaluronic Acid as a Modern Approach in Anticancer Therapy-Review. *Int. J. Mol. Sci.* **2023**, *24*, 103, https://doi.org/10.3390/ijms24010103.

Publisher's Note & Disclaimer

Supporting Materials

Table S01. 33 Different Cancer Types.

Serial No.	Name of Cancers (Short Form)	Name of Cancers (Full Form)
01	ACC	Adrenocortical carcinoma
02	BLCA	Bladder urothelial carcinoma
03	BRCA	Breast invasive carcinoma
04	CESC	Cervical squamous cell carcinoma and endocervical adenocarcinoma
05	CHOL	Cholangiocarcinoma
06	COAD	Colon adenocarcinoma
07	DLBC	Diffuse large B-cell lymphoma
08	ESCA	Esophageal carcinoma
09	GBM	Glioblastoma Multiforme
10	HNSC	Head and neck squamous cell carcinoma
11	KICH	Kidney Chromophobe
12	KIRC	Kidney renal clear cell carcinoma
13	KIRP	Kidney renal papillary cell carcinoma
14	LAML	Acute myeloid leukemia
15	LGG	Lower-grade glioma
16	LIHC	Liver hepatocellular carcinoma
17	LUAD	Lung adenocarcinoma
18	LUSC	Lung squamous cell carcinoma
19	MESO	Mesothelioma
20	OV	Ovarian serous cystadenocarcinoma
21	PAAD	Pancreatic adenocarcinoma
22	PCPG	Pheochromocytoma and Paraganglioma
23	PRAD	Prostate adenocarcinoma
24	READ	Rectum adenocarcinoma
25	SARC	Sarcoma
26	SKCM	Skin cutaneous melanoma
27	STAD	Stomach adenocarcinoma
28	TGCT	Testicular germ cell tumors
29	THCA	Thyroid carcinoma
30	THYM	Thymoma
31	UCEC	Uterine corpus endometrial carcinoma
32	UCS	Uterine Carcinosarcoma
33	UVM	Uveal melanoma

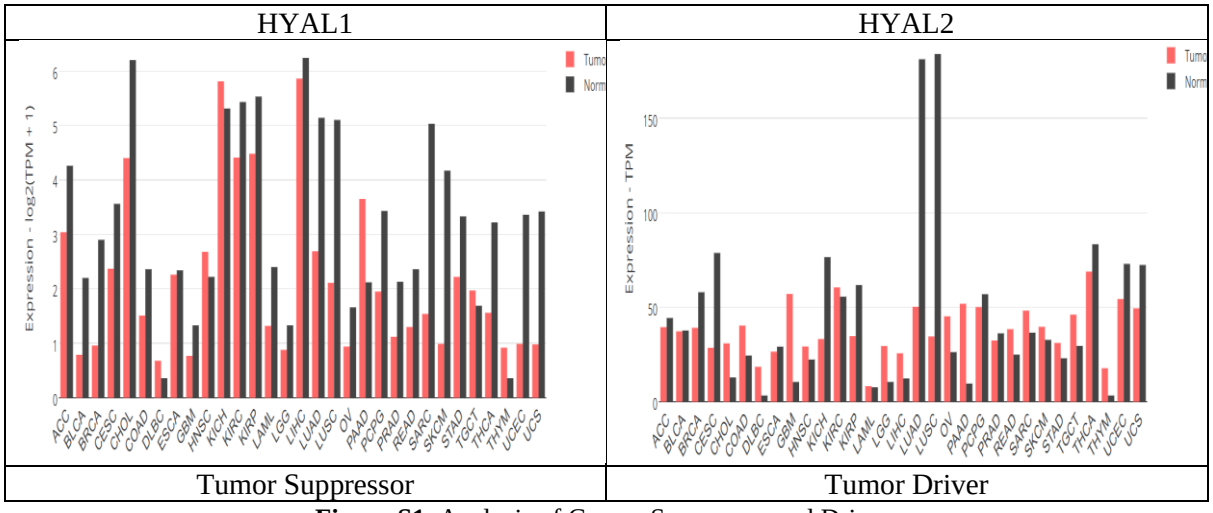

Figure S1. Analysis of Cancer Suppressor and Driver.

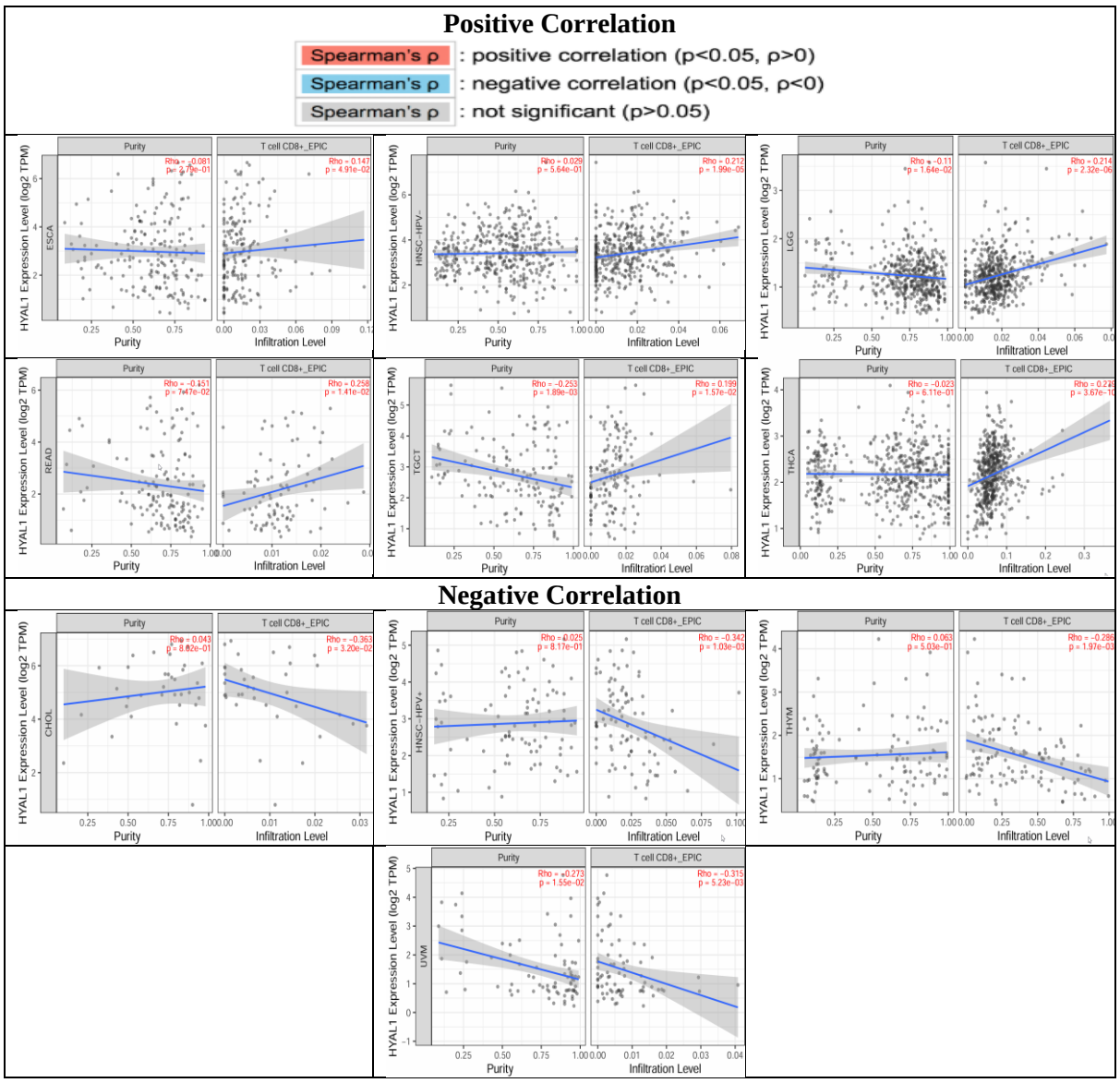

Figure S2. The correlation of HYAL1 expression with immune infiltration level in diverse cancer types.

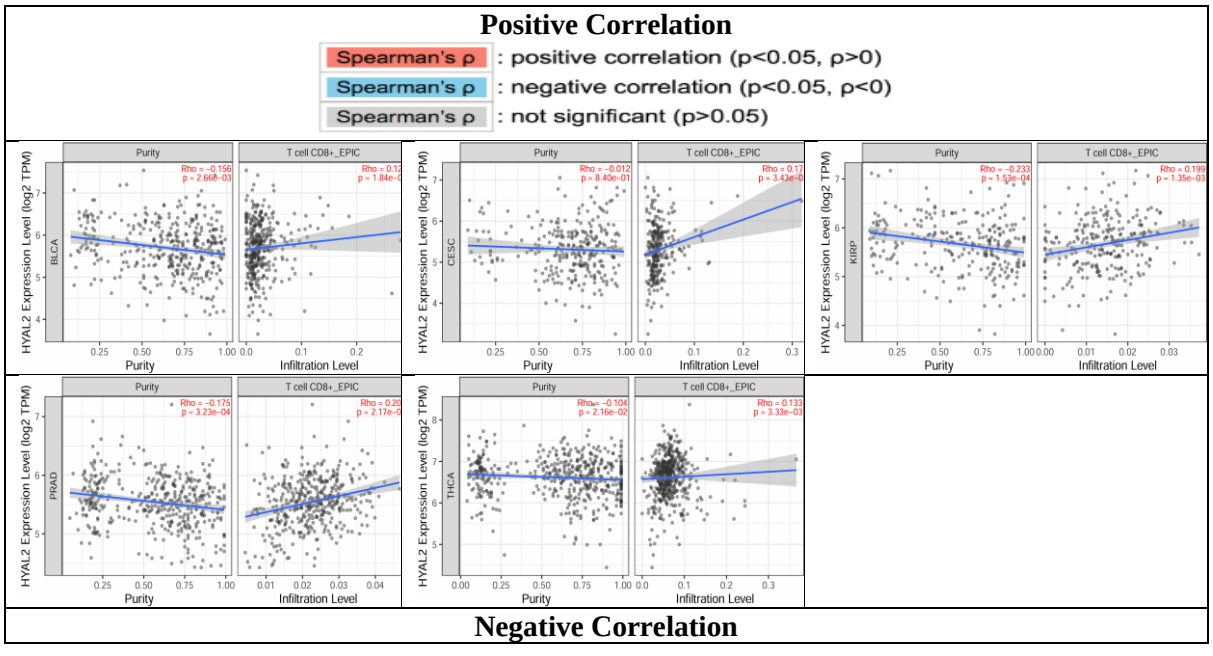

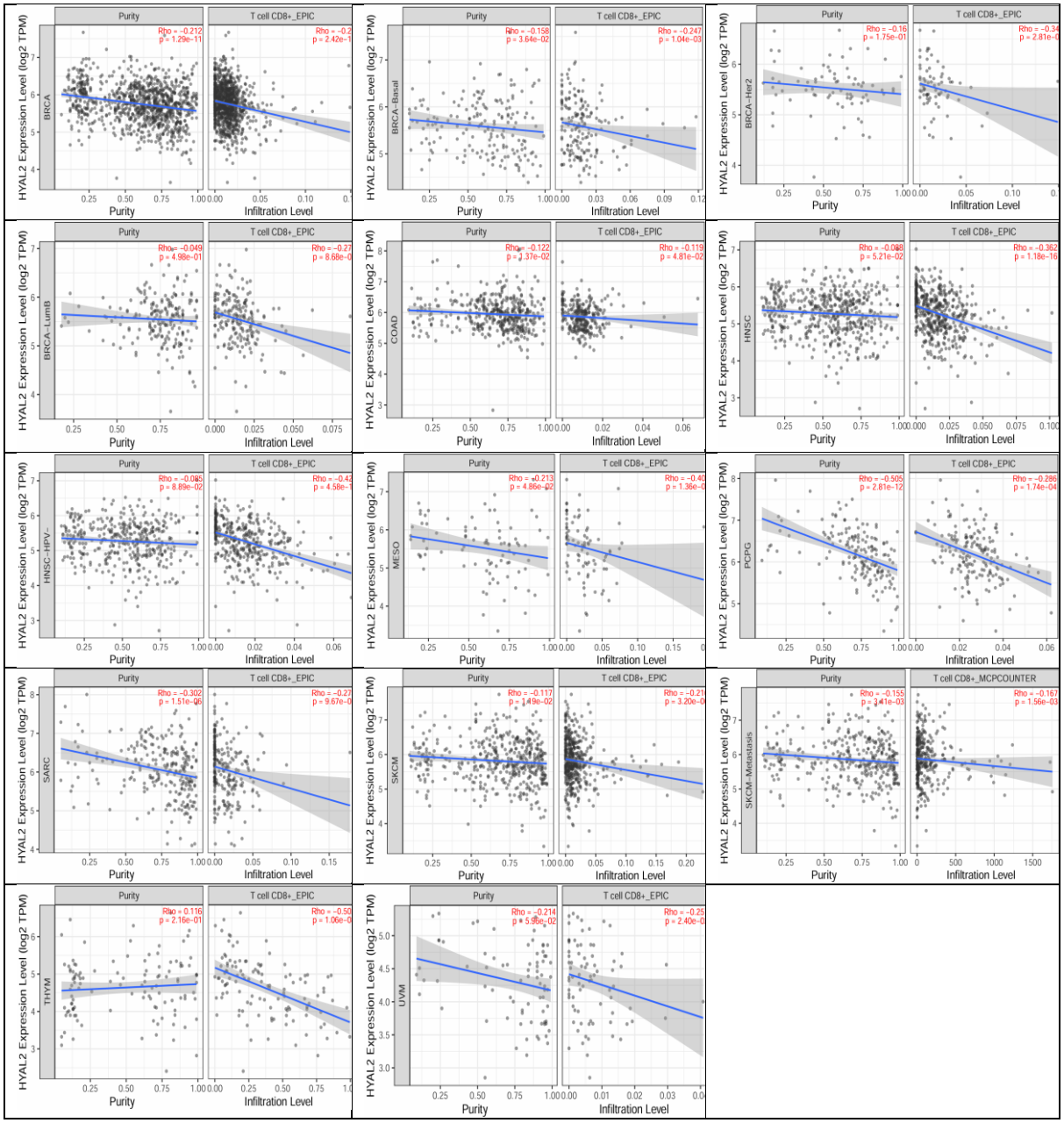

Figure S3. The correlation of HYAL2 expression with immune infiltration level in diverse cancer types.

Table S2. Molecular Docking Results.

HYAL1 Docking Results		**HYAL2 Docking Results**	
Compound	**XP glide Score (kcal/mol)**	**Compound**	**XP glide Score (kcal/mol)**
CHEMBL1200507	-10.775	CHEMBL1200455	-9.352
CHEMBL1200647	-10.381	CHEMBL1200455	-9.067
CHEMBL1095607	-9.65	CHEMBL1201075	-8.868
CHEMBL2104771	-9.65	CHEMBL1201202	-8.86
CHEMBL1200507	-9.431	CHEMBL1201075	-8.679
CHEMBL1200507	-9.425	CHEMBL1200455	-8.561
CHEMBL1200555	-8.647	CHEMBL1200614	-8.443
CHEMBL1278	-8.373	CHEMBL58	-8.046
CHEMBL1200601	-8.373	CHEMBL2364623	-7.856
CHEMBL58	-8.271	CHEMBL1650559	-7.856
CHEMBL1200556	-8.097	CHEMBL2364623	-7.796
CHEMBL1200647	-8.048	CHEMBL1650559	-7.796
CHEMBL2028852	-7.928	CHEMBL1200647	-7.644
CHEMBL1200647	-7.792	CHEMBL1725	-7.439
CHEMBL4650273	-7.668	CHEMBL1200455	-7.165
CHEMBL1200647	-7.623	CHEMBL1200614	-6.73
CHEMBL2028850	-7.494	CHEMBL1201075	-6.716

HYAL1 Docking Results		HYAL2 Docking Results	
Compound	**XP glide Score (kcal/mol)**	**Compound**	**XP glide Score (kcal/mol)**
CHEMBL1200555	-7.416	CHEMBL1200647	-6.57
CHEMBL329522	-7.36	CHEMBL1725	-6.485
CHEMBL345524	-7.268	CHEMBL4650273	-6.479
CHEMBL1007	-7.144	CHEMBL1007	-6.436
CHEMBL442	-6.866	CHEMBL1200614	-6.389
CHEMBL2448612	-6.866	CHEMBL2364623	-6.307
CHEMBL1185	-6.851	CHEMBL1650559	-6.307
CHEMBL3545184	-6.694	CHEMBL1725	-6.291
CHEMBL3545183	-6.694	CHEMBL1174	-6.203
CHEMBL3936761	-6.622	CHEMBL1201075	-6.188
CHEMBL1200647	-6.621	CHEMBL2364623	-6.157
CHEMBL4650273	-6.616	CHEMBL1650559	-6.157
CHEMBL372795	-6.557	CHEMBL1201202	-6.125
CHEMBL3184791	-6.557	CHEMBL1725	-6.11
CHEMBL372795	-6.534	CHEMBL1200647	-6.003
CHEMBL3184791	-6.534	CHEMBL1200647	-5.766
CHEMBL3833319	-6.516	CHEMBL2221250	-5.674
CHEMBL30008	-6.387	CHEMBL2221250	-5.593
CHEMBL3989909	-6.38	CHEMBL4650273	-5.537
CHEMBL3643413	-6.38	CHEMBL2221250	-5.441
CHEMBL1200501	-6.362	CHEMBL1429	-5.397
CHEMBL714	-6.351	CHEMBL1200556	-5.397
CHEMBL3989693	-6.351	CHEMBL2221250	-5.283
CHEMBL1441059	-6.351	CHEMBL2103929	-5.261
CHEMBL1002	-6.351	CHEMBL1200647	-5.215
CHEMBL1200517	-6.165	CHEMBL1201199	-5.171
CHEMBL1200517	-6.147	CHEMBL2068408	-5.053
CHEMBL1200555	-6.037	CHEMBL2364623	-5.002
CHEMBL2110824	-5.976	CHEMBL1650559	-5.002
CHEMBL1200501	-5.79	CHEMBL2104771	-4.976
CHEMBL1200454	-5.774	CHEMBL1201199	-4.974
CHEMBL5315123	-5.755	CHEMBL477	-4.928
CHEMBL1200854	-5.739	CHEMBL2104771	-4.927
CHEMBL1654	-5.582	CHEMBL3544973	-4.891
CHEMBL2104771	-5.54	CHEMBL938	-4.889
CHEMBL1095607	-5.54	CHEMBL1200501	-4.88
CHEMBL1654	-5.527	CHEMBL1200647	-4.871
CHEMBL1007	-5.503	CHEMBL1201112	-4.818
CHEMBL4594231	-5.461	CHEMBL1095607	-4.814
CHEMBL1615487	-5.461	CHEMBL1095607	-4.755
CHEMBL924	-5.446	CHEMBL354541	-4.712
CHEMBL4303669	-5.446	CHEMBL2105662	-4.712
CHEMBL1121	-5.393	CHEMBL467	-4.707
CHEMBL2096631	-5.382	CHEMBL2110824	-4.683
CHEMBL1213252	-5.382	CHEMBL938	-4.674
CHEMBL354541	-5.376	CHEMBL1643	-4.635
CHEMBL2105662	-5.376	CHEMBL1167	-4.568
CHEMBL1200555	-5.365	CHEMBL4802223	-4.527
CHEMBL3237547	-5.328	CHEMBL1200647	-4.478
CHEMBL923	-5.327	CHEMBL345714	-4.442
CHEMBL923	-5.303	CHEMBL3545184	-4.424
CHEMBL1200448	-5.261	CHEMBL3545183	-4.398
CHEMBL254857	-5.213	CHEMBL501122	-4.383
CHEMBL3833319	-5.124	CHEMBL2110824	-4.317
CHEMBL59	-5.094	CHEMBL3989403	-4.248
CHEMBL1557	-5.094	CHEMBL19490	-4.248
CHEMBL997	-5.087	CHEMBL938	-4.155
CHEMBL1200448	-5.086	CHEMBL2364608	-4.143
CHEMBL1624126	-5.083	CHEMBL2103929	-4.113
CHEMBL1560089	-5.083	CHEMBL3833319	-4.111
CHEMBL714	-5.07	CHEMBL2105950	-4.051
CHEMBL1441059	-5.07	CHEMBL1082	-4.051
CHEMBL3989806	-5.062	CHEMBL1637	-3.985
CHEMBL1200350	-5.062	CHEMBL4650273	-3.958

HYAL1 Docking Results		HYAL2 Docking Results	
Compound	**XP glide Score (kcal/mol)**	**Compound**	**XP glide Score (kcal/mol)**
CHEMBL1165268	-5.062	CHEMBL42403	-3.936
CHEMBL502135	-5.053	CHEMBL1167	-3.915
CHEMBL2107355	-5.013	CHEMBL3237547	-3.895
CHEMBL502135	-5.004	CHEMBL4802223	-3.862
CHEMBL2107826	-4.948	CHEMBL1460	-3.809
CHEMBL354541	-4.925	CHEMBL2110824	-3.8
CHEMBL2105662	-4.925	CHEMBL1200647	-3.653
CHEMBL2103844	-4.888	CHEMBL4802223	-3.639
CHEMBL167731	-4.888	CHEMBL1464	-3.627
CHEMBL1200454	-4.817	CHEMBL1200879	-3.627
CHEMBL1624126	-4.812	CHEMBL1200772	-3.627
CHEMBL1560089	-4.812	CHEMBL3545184	-3.589
CHEMBL3989798	-4.792	CHEMBL3545183	-3.589
CHEMBL1256786	-4.792	CHEMBL888	-3.512
CHEMBL939	-4.792	CHEMBL43452	-3.42
CHEMBL3989798	-4.726	CHEMBL1357	-3.386
CHEMBL1256786	-4.726	CHEMBL1200747	-3.386
CHEMBL834	-4.672	CHEMBL2374220	-3.372
CHEMBL1200380	-4.647	CHEMBL2221250	-3.367
CHEMBL3989798	-4.633	CHEMBL1397	-3.366
CHEMBL1256786	-4.633	CHEMBL1357	-3.354
CHEMBL3833327	-4.616	CHEMBL1200747	-3.354
CHEMBL1556	-4.616	CHEMBL3301605	-3.353
CHEMBL345524	-4.614	CHEMBL3112741	-3.353
CHEMBL834	-4.611	CHEMBL1201129	-3.242
CHEMBL1201042	-4.605	CHEMBL1200647	-3.176
CHEMBL871	-4.583	CHEMBL1201129	-3.166
CHEMBL924	-4.531	CHEMBL3833327	-3.139
CHEMBL4303669	-4.531	CHEMBL1556	-3.139
CHEMBL1750	-4.531	CHEMBL3187723	-3.119
CHEMBL1624126	-4.516	CHEMBL2105754	-3.1
CHEMBL1560089	-4.516	CHEMBL1650443	-3.1
CHEMBL2062263	-4.46	CHEMBL1167	-3.014
CHEMBL927	-4.453	CHEMBL43452	-3.012
CHEMBL554	-4.373	CHEMBL1200517	-2.997
CHEMBL1201179	-4.373	CHEMBL3833319	-2.97
CHEMBL2096631	-4.366	CHEMBL2103929	-2.938
CHEMBL1213252	-4.366	CHEMBL1200517	-2.931
CHEMBL1201129	-4.328	CHEMBL3137333	-2.921
CHEMBL1533310	-4.278	CHEMBL1183349	-2.921
CHEMBL2110824	-4.25	CHEMBL602	-2.916
CHEMBL1201042	-4.242	CHEMBL1256137	-2.916
CHEMBL2096646	-4.239	CHEMBL1464	-2.835
CHEMBL1200584	-4.239	CHEMBL1200879	-2.835
CHEMBL997	-4.238	CHEMBL1200772	-2.835
CHEMBL871	-4.23	CHEMBL354541	-2.825
CHEMBL1201112	-4.201	CHEMBL2105662	-2.825
CHEMBL1697760	-4.138	CHEMBL3989756	-2.803
CHEMBL3989798	-4.06	CHEMBL3833314	-2.803
CHEMBL1256786	-4.06	CHEMBL3185229	-2.803
CHEMBL1200454	-4.048	CHEMBL938	-2.761
CHEMBL5314375	-4.014	CHEMBL2221250	-2.716
CHEMBL152	-4.014	CHEMBL1200380	-2.685
CHEMBL2062263	-4.012	CHEMBL2364623	-2.667
CHEMBL1800159	-4.006	CHEMBL1650559	-2.667
CHEMBL277100	-3.995	CHEMBL3137333	-2.593
CHEMBL2107495	-3.995	CHEMBL1183349	-2.593
CHEMBL2079793	-3.939	CHEMBL3545367	-2.582
CHEMBL1200854	-3.926	CHEMBL3833319	-2.404
CHEMBL997	-3.899	CHEMBL2105950	-2.383
CHEMBL2048028	-3.879	CHEMBL1082	-2.383
CHEMBL1201016	-3.853	CHEMBL2103929	-2.375
CHEMBL1043	-3.846	CHEMBL3137333	-2.338
CHEMBL1201319	-3.816	CHEMBL1183349	-2.338

HYAL1 Docking Results		HYAL2 Docking Results	
Compound	**XP glide Score (kcal/mol)**	**Compound**	**XP glide Score (kcal/mol)**
CHEMBL744	-3.798	CHEMBL1200647	-2.318
CHEMBL43452	-3.754	CHEMBL1200501	-2.304
CHEMBL4297067	-3.669	CHEMBL3137333	-2.148
CHEMBL1200454	-3.659	CHEMBL1183349	-2.148
CHEMBL1201198	-3.656	CHEMBL2221250	-2.115
CHEMBL1201050	-3.656	CHEMBL1697844	-2.115
CHEMBL4535757	-3.627	CHEMBL938	-2.113
CHEMBL713	-3.56	CHEMBL2103929	-2.082
CHEMBL5314362	-3.56	CHEMBL1103	-2.069
CHEMBL1697760	-3.547	CHEMBL3833322	-2.053
CHEMBL2068408	-3.535	CHEMBL1460	-1.92
CHEMBL1095	-3.518	CHEMBL2104771	-1.809
CHEMBL5314375	-3.507	CHEMBL1095607	-1.809
CHEMBL152	-3.507	CHEMBL1201129	-1.809
CHEMBL2096633	-3.499	CHEMBL3304485	-1.706
CHEMBL3989939	-3.496	CHEMBL3301627	-1.706
CHEMBL3889654	-3.496	CHEMBL1007	-1.682
CHEMBL1200670	-3.495	CHEMBL2221250	-1.675
CHEMBL43452	-3.472	CHEMBL3304485	-1.665
CHEMBL1624126	-3.441	CHEMBL3301627	-1.665
CHEMBL1560089	-3.441	CHEMBL3833319	-1.656
CHEMBL830	-3.437	CHEMBL3137309	-1.576
CHEMBL1583	-3.436	CHEMBL1200879	-1.475
CHEMBL1200965	-3.436	CHEMBL1200772	-1.475
CHEMBL2219738	-3.431	CHEMBL1464	-1.423
CHEMBL2107168	-3.431	CHEMBL3137333	-1.218
CHEMBL2105248	-3.431	CHEMBL1183349	-1.218
CHEMBL2062263	-3.431	CHEMBL1167	-1.091
CHEMBL3833319	-3.408	CHEMBL1200501	-1.085
CHEMBL997	-3.365	CHEMBL3187723	-1.03
CHEMBL468	-3.337	CHEMBL1200879	-0.986
CHEMBL468	-3.326	CHEMBL1200772	-0.986
CHEMBL1177	-3.29	CHEMBL1464	-0.985
CHEMBL1757	-3.27	CHEMBL1397	-0.966
CHEMBL861	-3.254	CHEMBL2374220	-0.948
CHEMBL1201000	-3.252	CHEMBL3137333	-0.866
CHEMBL379845	-3.244	CHEMBL1183349	-0.866
CHEMBL488	-3.222	CHEMBL3304485	-0.856
CHEMBL1278	-3.217	CHEMBL3301627	-0.856
CHEMBL1200601	-3.217	CHEMBL2104771	-0.846
CHEMBL960	-3.206	CHEMBL1095607	-0.846
CHEMBL3833319	-3.183	CHEMBL3137333	-0.798
CHEMBL1624126	-3.048	CHEMBL1183349	-0.798
CHEMBL1560089	-3.048	CHEMBL3833319	-0.602
CHEMBL861	-3.036	CHEMBL888	-0.538
CHEMBL1100	-3.022	CHEMBL1637	-0.538
CHEMBL1201016	-3.0	CHEMBL3833319	-0.289
CHEMBL4297067	-2.984	CHEMBL1200517	-0.217
CHEMBL9	-2.963	CHEMBL2374220	-0.19
CHEMBL843	-2.893	CHEMBL2374220	-0.116
CHEMBL121	-2.893	CHEMBL3304485	-0.093
CHEMBL1014	-2.85	CHEMBL3301627	-0.093
CHEMBL1103	-2.825	CHEMBL602	0.098
CHEMBL1229517	-2.817	CHEMBL1256137	0.098
CHEMBL254857	-2.803	CHEMBL938	0.099
CHEMBL826	-2.799	CHEMBL2374220	0.272
CHEMBL1095	-2.799	CHEMBL3833319	0.32
CHEMBL488	-2.784	CHEMBL467	0.407
CHEMBL1177	-2.77	CHEMBL1200517	0.484
CHEMBL29411	-2.694	CHEMBL2374220	0.619
CHEMBL1177	-2.652	CHEMBL2374220	0.798
CHEMBL695	-2.638	CHEMBL1201202	1.04
CHEMBL277100	-2.571	CHEMBL3833319	1.139
CHEMBL2107495	-2.571	CHEMBL602	1.408

HYAL1 Docking Results		HYAL2 Docking Results	
Compound	**XP glide Score (kcal/mol)**	**Compound**	**XP glide Score (kcal/mol)**
CHEMBL345714	-2.524	CHEMBL1256137	1.408
CHEMBL830	-2.52	CHEMBL2374220	1.582
CHEMBL1624126	-2.505	CHEMBL1007	1.603
CHEMBL1560089	-2.505	CHEMBL3137309	1.753
CHEMBL1757	-2.468	CHEMBL2374220	1.974
CHEMBL1177	-2.334	CHEMBL1201199	2.225
CHEMBL843	-2.322	CHEMBL1200517	2.534
CHEMBL121	-2.322	CHEMBL3137333	2.571
CHEMBL4297067	-2.301	CHEMBL1183349	2.571
CHEMBL573	-2.256	CHEMBL3304485	2.99
CHEMBL1909285	-2.184	CHEMBL3301627	2.99
CHEMBL3989756	-2.174	CHEMBL501122	9.76
CHEMBL3833314	-2.174	CHEMBL3544973	9.76
CHEMBL3185229	-2.174		
CHEMBL1100	-2.1		
CHEMBL1200751	-1.969		
CHEMBL1425	-1.896		
CHEMBL1200751	-1.784		
CHEMBL1425	-1.755		
CHEMBL1583	-1.614		
CHEMBL1200965	-1.614		
CHEMBL90	-1.383		
CHEMBL3989520	-1.383		
CHEMBL90	-1.295		
CHEMBL3989520	-1.295		
CHEMBL1533310	-1.295		
CHEMBL416	-1.149		
CHEMBL455	-0.286		
CHEMBL1014	0.452		
CHEMBL2028852	1.493		
CHEMBL2028850	1.493		